Climate Dynamics (2020) 54:413–433
https://doi.org/10.1007/s00382-019-05005-7

ENSO diversity and the recent appearance of Central Pacific ENSO

Ying Feng[1,2] · **Xianyao Chen**[3] · **Ka-Kit Tung**[2]

Received: 11 February 2019 / Accepted: 1 October 2019 / Published online: 10 October 2019
© Springer-Verlag GmbH Germany, part of Springer Nature 2019

Abstract
ENSO diversity refers to the appearance in recent decades of different El Niño types in the tropical Pacific: In addition to the canonical El Niño, the newly discovered type, called Central Pacific (CP) El Niño, has its center of warming shifted more to the central equatorial Pacific. Whether these ENSO types are really distinct or are different manifestations of a continuum is currently under debate. The mechanisms for the recent appearance of the additional type of ENSO have not been clarified. While previously it was claimed that the increased CP El Niño occurrence in recent decades were due to tropical trade winds weakened by global warming, the observed trade winds actually intensified. We systematically study the variability of the Pacific sea-surface temperature (SST) using the new method of Rotated Principal Component Analysis (RPCA). The essential statistical characteristics of these two El Niño types are found to be describable by only three fundamental modes of pan-Pacific SST with different proportions: the ENSO-cycle, the pan-Pacific counterpart of the regionally defined Pacific Decadal Oscillation (PDO), and a new climate mode we call the Central Pacific Variability (CPV). It is shown that CP El Niño can be described by the PDO and the CPV. The latter has a horseshoe-shaped warm SST pattern in the Central Pacific flanked by cold SST to the east, roughly similar to the original definition of ENSO Modoki by Ashok et al. (J Geophys Res Oceans 112:C11007, 2007) as the second Empirical Orthogonal Function in a narrow tropical domain decomposition. The Principal Component (PC) of this mode, called Modoki PC (MPC) was thought to characterize the occurrence of this new phenomenon, but it has been shown to be unable to separate it from the canonical ENSO. In contrast, we demonstrate that Central Pacific El Niño occurs when the CPV index is larger than 0.5. The intensity of the CPV mode has increased dramatically since 1970s, likely as a result of the intensification of the easterly trade winds in the tropical Pacific, which tilts the thermocline along the tropical Pacific and raises the SST in the central equatorial Pacific. Moderate El Niños are more prone to stalling in the Central Pacific, becoming CP El Niños.

Keywords ENSO Modoki · Central Pacific El Niño · ENSO diversity · Trade wind intensification

1 Introduction

Two well-known climate modes of SST variability in the Pacific are: El Niño-Southern Oscillation (ENSO) (Philander 1983; Glantz and Glantz 2001; Sarachik and Cane, 2010) in the tropical Pacific and the Pacific Decadal Oscillation (PDO) in the North Pacific (Mantua et al. 1997). These modes can be obtained as the leading mode in an Empirical Orthogonal Function (EOF) expansion of the SST in the tropical Pacific, and North Pacific (north of 20°N), respectively. It has become increasingly clear that these two modes are not sufficient to describe the diversity of phenomena associated with SST variability observed in the Pacific basin, the largest of the world's oceans.

A second mode of SST variability in the tropical Pacific has been noticed recently in the data analyzed for the recent 3 decades. This mode is like the canonical El Niño but with the center of maximum SST warming shifted to the Central Pacific. It is called variously as "El Niño Modoki" (Ashok et al. 2007, Ashok and Yamagata 2009), "Date line El Niño" (Larkin and Harrison 2005a, b), "Central-Pacific El Niño" (Kao and Yu 2009), or "Warm Pool El Niño" (Kug

✉ Ka-Kit Tung
ktung@uw.edu

[1] College of Ocean and Earth Sciences, Xiamen University, Xiamen, China

[2] Department of Applied Mathematics, University of Washington, Seattle, WA, USA

[3] Key Laboratory of Physical Oceanography, Ocean University of China, and Qingdao National Laboratory of Marine Science and Technology, Qingdao, China

et al. 2009). Despite different names, these studies basically describe the same phenomenon. We shall adopt the name CP El Niño in this paper. Canonical El Niño event is now referred to as Eastern Pacific (EP) El Niño (Kao and Yu 2009). It is also called cold tongue El Niño (Kug et al. 2009). We shall use the name EP El Niño in this paper except when reviewing other authors' results.

There were also several statistical definitions. The first such definition was by Ashok et al. 2007 as the second EOF of Pacific SST anomaly restricted to the tropical latitudes in the SST data during 1979–2005, with the first EOF being the canonical ENSO. This definition is still commonly used. Kao and Yu (2009) argued that these two EOF modes contain signal from Niño 1 + 2 and Niño 4 regions and therefore cannot accurately describe the main characteristics of the new type of ENSO events. They proposed to first regress out the Niño 1 + 2 index from the SST before performing the tropical EOF analysis to define the CP ENSO. Similarly, Niño 4 signal is removed before EOF analysis when they obtain the EP El Niño as the first EOF. Kug et al. (2009) classified the two types of El Niño by comparing SST anomaly in Niño 3 and Niño 4 regions. When the larger SST anomaly is in Niño 3 region, they called it Cold Tongue El Niño. When the maximum SST anomaly is located in Niño 4 region, it is classified as Warm Pool El Niño. Ren and Jin (2011) obtained their index for the new type of El Niño by nonlinearly transforming the Niño 3 and Niño 4 indices.

Yu et al. (2012) classified El Niño events from 1950 on into CP and EP El Niño using three criteria: the EP/CP method of Kao and Yu (2009), the Niño 3/Niño 4 method of Kug et al. (2009), and the EMI method of Ashok et al. (2007, Ashok and Yamagata 2009). (The EMI index is defined in the next paragraph.)

The two regional modes in the tropical Pacific are shown in the top row of Fig. 1. The first tropical EOF is the "canonical" ENSO mode, while the second EOF was used to define the Modoki mode by Ashok et al. (2007), and its PC is used as a Modoki Index (called the MPC index). This second mode has a horseshoe-shaped warm region in the Central Pacific flanked by cold eastern and western Pacific SST oriented along the Equator. The green rectangles in the top right panel of Fig. 1 indicate the areas of contrasting SSTs that were thought to characterize the Modoki mode, and used to define the ENSO Modoki Index (EMI). As we expand the artificial boundary in other panels of Fig. 1, it is seen that the second EOF is not robust, being highly dependent on the meridional domain used. In the larger domains, the second EOF no longer shows the contrast between the regions highlighted by the green boxes in the limited domain.

Ashok et al. (2007)'s EOF analysis was performed on a tropical domain 30°S–30°N. There has been a tendency for subsequent authors to use even narrower domains. For example the tropical domain of 20°S–20°N was used by Yeh et al.

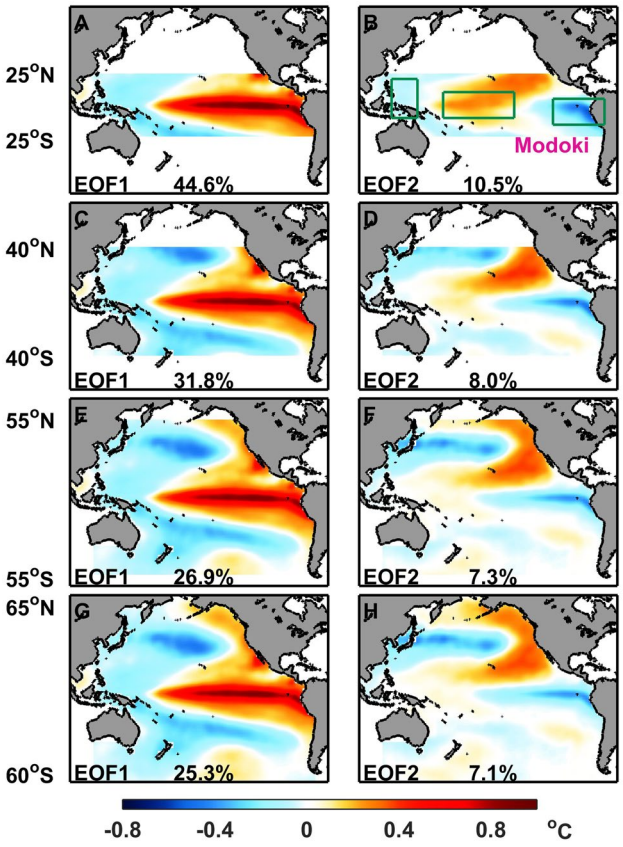

Fig. 1 Regional versus pan-Pacific EOF expansion of SST. The first (left column) and second (right column) EOF modes are shown for domains restricted to, from top to bottom: 25°N–25°S, 40°N–40°S, 55°N–55°S and 65°N–60°S, respectively

(2009), 15°S–15°N by Cai et al. (2015), and 10°S–10°N by Takahashi et al. (2011). Takahashi et al. (2011) found that the Principal Component (PC) associated with the Modoki mode of Ashok et al. (2007) is not robust with respect to the periods analyzed. Robustness of both the spatial structure and its PC was found for a narrower domain 10°S–10°N. Ashok et al. (2007) mentioned that the Modoki mode exists in a domain even as narrow as 5°S–5°N. A question arises as to whether such a "robust" structure, which Ashok et al. called a tripole, is an artifact due to the elimination of meridional variation in a narrow domain and its effect on the EOF analysis. That is, a narrow domain confines the EOF spatial patterns to mostly one-dimensional variations along the Equator. Perhaps it is similar to the one-dimensional Fourier decomposition of 1 into odd sines: sinx (monopole), sin3x (tripole), etc.? If so, the individual modes should not be given physical interpretation.

EOF analysis performed on a restricted domain is prone to a mathematical artifact called Buell patterns (Buell 1979; North et al. 1982). Using a synthetic example of a tropical ENSO shape, a structure of one sign, decomposed into

orthogonal EOFs in 30°S–30°N, Lian and Chen (2012) showed that the EOF analysis would tend to create monopole and tripole etc. structures oriented along the equator to satisfy the orthogonality constraint in the narrow domain of the tropical Pacific. The first mode, a monopole, looks like the canonical El Niño, while the second mode is a tripole (which they somehow called a "dipole"). The "Modoki" mode has a structure similar to the tripole mode. It is clearly artificial in this example because the original input function does not change sign along the Equator. Lian and Chen (2012) concluded: "despite the newly aroused interest in El Niño Modoki, the dipole structure of this mode is not likely to be a truthful representation of the real climate variability". Nevertheless, this demonstration does not necessarily imply that the "Modoki" mode is an artifact, since a number of studies have also been able to identify the typical Modoki events [see the review paper from Capotondi et al. (2015)] based on the SST indices, which are independent of EOF methods. However, the search for the cause or mechanism of the Modoki phenomenon is hampered by its mathematical definition that changes shape when the artificial northern and southern boundaries are moved. Partly as a result, no consensus has emerged on the physical mechanism involved although a large number of proposals have been advanced in recent literature.

More than a dozen indices have been created to represent the diversity of the ENSO phenomena in the tropical Pacific, seven of which were reviewed in Capotondi et al. (2015), and three used by Yu et al. (2012) as criteria for classification. These indices are ad hoc and not necessarily orthogonal. Although physically defined indices do not need to be orthogonal, they may not be efficient in that they may overlap in the phenomenon they represent. For example, as we will show, these indices can be distilled into a much smaller number, with different indices being merely different combinations of three fundamental modes. Four modes are sufficient to represent most of the variance in the Pacific. The fourth mode is needed for representing the extratropical North Pacific variability adequately, but its variance in the tropical Pacific is minimal. The reported "regime change" of EP ENSO to CP ENSO is investigated using the other three fundamental modes. Only two of these modes show "regime change" behavior: the PDO and a Central Pacific horseshoe-shaped mode, called the Central Pacific Variability (CPV) here. The former has been going through its quasi-periodic multidecadal phase shifts, experiencing a positive phase between 1976 and 1998, and then a negative phase; the latter shows a secularly increasing variance since 1970s, possibly in response to the intensification of Pacific trade winds, as will be discussed later.

The perceived importance of this new type of El Niño, the CP El Niño, derives from its projected change under anthropogenic warming. Yeh et al. (2009) found that for the period 1854–2007, the frequency of occurrence of CP El Niño increased from 0.01 per year before 1990 to 0.29 per year after 1990, and suggested that it will increase even more under future warming scenarios, by as much as five times. The mechanism of the increase in frequency of occurrences was proposed to be due to the flattening of the thermocline in the Central Pacific, caused by the weakening of the trade winds in coupled climate models. Lee and McPhaden (2010) pointed out that that proposed mechanism could not explain another important fact of the CP El Niño, that is, its intensity has doubled from 1982 to 2010 in observation, but not in models. McPhaden et al. (2011) and Xiang et al. (2013) showed evidence that the observed thermocline tilt actually steepened instead of flattened. Cai et al. (2015) pointed that the model projected slowdown in Walker circulation under global warming should boost instead the occurrence of eastward propagating warm SST anomaly that characterize extreme EP El Niño events. They noted the "stark contrast" between model and observation, with the latter showing that the Walker circulation strengthened during the last 3 decades.

One notable discrepancy between observation and the coupled climate models is the intensification of the tropical Pacific trade wind since at least 1979 in the mean state (Fedorov et al. 2015). See Fig. 9 later. The trade winds are easterly, which normally tend to inhibit the development of the EP El Niño unless the latter is preceded by a westerly wind burst of sufficient strength. Thus it is reasonable to expect that as the trade winds intensified for the past 3 decades in the mean state the development of the El Niño sometimes stalls in the Central Pacific, not reaching its canonical location of the Eastern Pacific. The stalled El Niño may appear like a "Standing Central Pacific Warming" (Xiang et al. 2013).

The SST data used in this paper is NOAA's Reconstructed Sea-Surface Temperature version 3b (ERSSTv3b) (Smith and Reynolds 2004; Smith et al. 2008). Surface wind stress is from ERA-interim monthly dataset (Dee et al. 2011), available since 1979. Subsurface temperature data are from Ishii (Ishii et al. 2005, 2006; Ishii and Kimoto 2009); 2012 is the last year that they are available. We merge them with Argo data available for 2004–2016. The two datasets are very consistent except that their means are different. During the period of overlap, the means of the two datasets are matched.

2 Regional versus pan-Pacific EOFs, and mode mixing

Many climate modes previously studied were defined through regional EOF analysis. In particular, the PDO was defined by Mantua et al. (1997) as the leading EOF of the

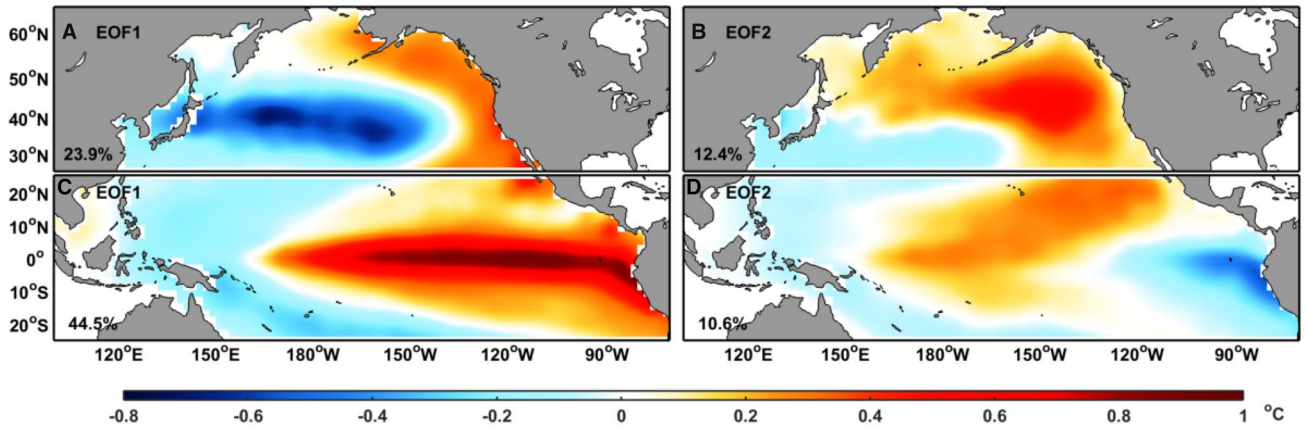

Fig. 2 Two leading EOFs of SST* in (top row) the north Pacific (north of 25°N); and (bottom row) tropical Pacific domain (25°S–25°N)

SST* in the Pacific north of 20°N, with an associated PC that is commonly used as the PDO Index. (SST* is defined as the SST with the global-mean SST subtracted at every grid-point.). Although a recent review (Newman et al. 2016) suggested that the PDO is caused by many different mechanisms, it is commonly regarded as a single physical climate mode, and not a statistical artifact. In Fig. 2, we show the first and second leading EOFs of SST* in the regions north of 25°N in the top row and the first and second leading EOFs in the tropical region 25°S–25°N. The use of 25°N instead of 20°N does not change the well-known shape of the PDO: a bullet-like cold region in the northwestern Pacific flanked by warm SST to the east, along the US coast, in its positive phase, and the reverse pattern in its negative phase. The artificial boundary for the EOF analysis is moved from 20°N to 25°N here to make the change across the boundary less abrupt. The second EOF in the extratropical Pacific (top right panel of Fig. 2) was named the Victoria mode (Ding et al. 2015), or the North Pacific Gyre Oscillation (Di Lorenzo et al. 2008) (though with respect to sea-surface heights).

The two leading EOFs of the tropical domain (lower panels) are thought to be the canonical ENSO and the ENSO Modoki modes (Ashok et al. 2007), and their PCs are often used as indices for the respective phenomenon. Neither is a pure ENSO index, as they both contain a substantial PDO component. After all, there is no real boundary between the extratropical and tropical Pacific in the observational data.

Takahashi et al. (2011), without mentioning the PDO, found that the increased occurrence of CP ENSO events is not along the Modoki PC (MPC) axis of Ashok et al. (2007), which is the second PC in the tropical domain:

> The classification of events into Central Pacific (Yeh et al. 2009) or Modoki (Ashok et al. 2007) El Niño can be shown in PC1-PC2 space (see caption of Fig. 1 for the criteria used in both cases), and we see that neither reflects a preferential clustering of climate states, so from this perspective there is no evidence that they depict a new type of phenomenon separate from ENSO, as argued by Ashok et al. (2007). Interestingly, the 'canonical' El Niño composite (Rasmusson and

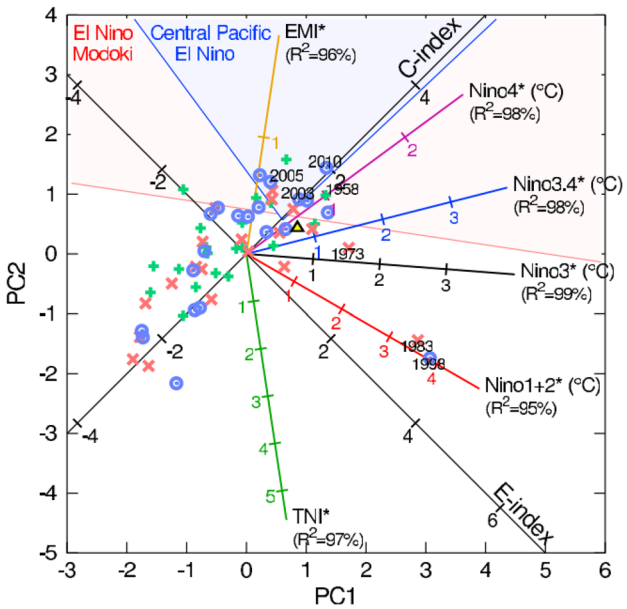

Fig. 3 Taken from Takahashi et al. (2011): December–February (DJF) mean PC1 and PC2 from HadISST (period 1950–1969: green plusses; 1970–1989: red crosses; 1990–2010: blue circles; Rasmusson and Carpenter's (1982) composite is shown in a yellow triangle). Also shown are the axes corresponding to different multiple-regression estimates of Niño indices (variance explained indicated), as well as the E and C axes. The light-blue and light-red areas approximately correspond to CP events following Yeh et al. (2009) (i.e. Niño 3* > 0.5 °C or Niño 4* > 0.5 °C, and Niño 4* > Niño 3*) and Modoki events following Ashok et al. (2007) (i.e. EMI* > 0.7 standard deviation of 1979–2004 DJF-mean EMI*)

Carpenter 1982) is closer to the Modoki category than to the two extraordinary El Niño events of 1982–1983 and 1997–1998, while the 'canonical' 1957–1958 event clearly classifies as Modoki.

As shown in their Fig. 1 (Fig. 3 here), the CP El Niño events occur along a 45° angle from the PC2 axis. The diagonal axis, which they called the C-axis, is formed by the sum of the two leading PCs of the narrow tropical domain. Similar to the pan-Pacific case discussed later by Chen and Wallace (2016), the 45° rotation largely removes the PDO component mixed in the first two PCs (more so in the pan-Pacific EOFs than in the tropical EOFs). However in the narrow tropical domain, the procedure at the same time also mixes Ashok et al. (2007)'s CP ENSO and canonical ENSO indices into the C axis, leading the authors to the interpretation quoted above. We will discover unmixed indices for both canonical and CP ENSOs in the pan-Pacific SST by rotating two pairs, instead of only one pair of PCs as was done by Takahashi et al. (2011). It turns out that tropical SST is expressible by three fundamental modes, ENSO-cycle, pan-Pacific PDO (pan-PDO) and another mode we term the Central Pacific Variability (CPV), in addition to the warming trend. The three components cannot be separated by rotating only one pair of PCs. Our results from two-pairs rotation are highlighted in Fig. 4. Justification will be given later. It is a 2-D plot of pair-wise rotated PCs: prPC4 versus prPC2. It is seen that the CP El Niño occurrences since 1950 (when the classification by Yu et al. (2012) began) are separated by prPC4 > 0.5. Previously there has not been a definitive criterion for the classification of CP El Niño. There are three separate criteria used by Yu et al. (2012) in classifying CP El Niño, and they sometimes disagree. In Fig. 4 we use the consensus criteria, i.e. when all three criteria agree that an event is CP El Niño. (Note that the word "consensus" was used perhaps incorrectly in Yu et al. (2012). They also called it "consensus" when 2 out of 3 agree in their Table 1. We call 2 out of 3 "majority" here.) Figure 4 shows that a single, definitive criterion for separating CP from EP El Niño is found in prPC4.

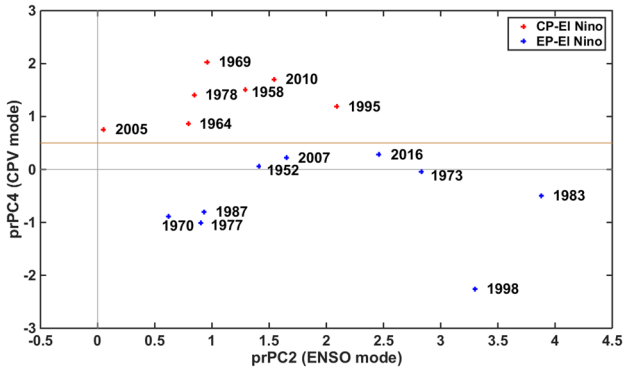

Fig. 4 El Niño occurrences plotted in prPC2–prPC4 plane. EOF analysis is performed on SST anomaly. Red crosses denote CP El Niño events and blue crosses EP El Niño event. The threshold prPC4 = 0.5 separates the two types of El Niño. El Niño occurrence is defined following NOAA's convention: when the Ocean Niño Index (ONI), which is the 3-month running mean of Niño 3.4 index, exceeds 0.5 °C for 5 consecutive months. Shown are 3-month average of the prPC values centered around the peak value. When an event spans two calendar years, only the second year is labeled. Note that the extraordinary EP El Niño 1997–1998 mentioned by Takahashi et al. (2011) is not separate from other EP El Niños, except that it has a more negative prPC4 value. This is explained in the text by the role of prPC4 on Niño 1 + 2

In Fig. 5, we expand the domain to pan Pacific, thus removing the artificial boundary at 25°N and 25°S. Conventional EOF analysis is performed. The leading pan-Pacific EOF, the so-called "ENSO-like" mode (Zhang et al. 1997), is seen to be a simple combination of the regional ENSO mode in the tropical Pacific and the regional PDO mode in the North Pacific. This is inevitable due to the requirement that the leading mode maximizes the variance explained in the larger domain, which necessarily includes the leading modes in the two smaller constituent domains. As a result, the leading pan-Pacific PC is a mix of the interannual

Table 1 The definition of some tropical indices based on SSTa data

Index	Latitude range	Longitude range	Method
Niño 1 + 2	0°–10°S	90°W–80°W	Area-averaged SSTa
Niño 3	5°N–5°S	150°W–90°W	Area-averaged SSTa
Niño 4	5°N–5°S	160°E–150°W	Area-averaged SSTa
Niño 3.4	5°N–5°S	170°W–120°W	Area-averaged SSTa
CTI	6°N–6°S	180°W–90°W	Area-averaged SST*
JMA	4°N–4°S	150°W–90°W	Area-averaged SSTa
Mega-ENSO	Eastern Pacific triangle–western Pacific K-Shape regions		Area-averaged SSTa
TNI	Normalized Niño 1 + 2–normalized Niño 4		Area-averaged SSTa
EMI	(10°N–10°S, 165°E–140°W) − 0.5 * [(5°N–15°S, 110°W–70°W) + (20°N–10°S, 125°E–145°E)]		Area-averaged SSTa
MPC	20°N–20°S	Pacific region	PC2 of SSTa

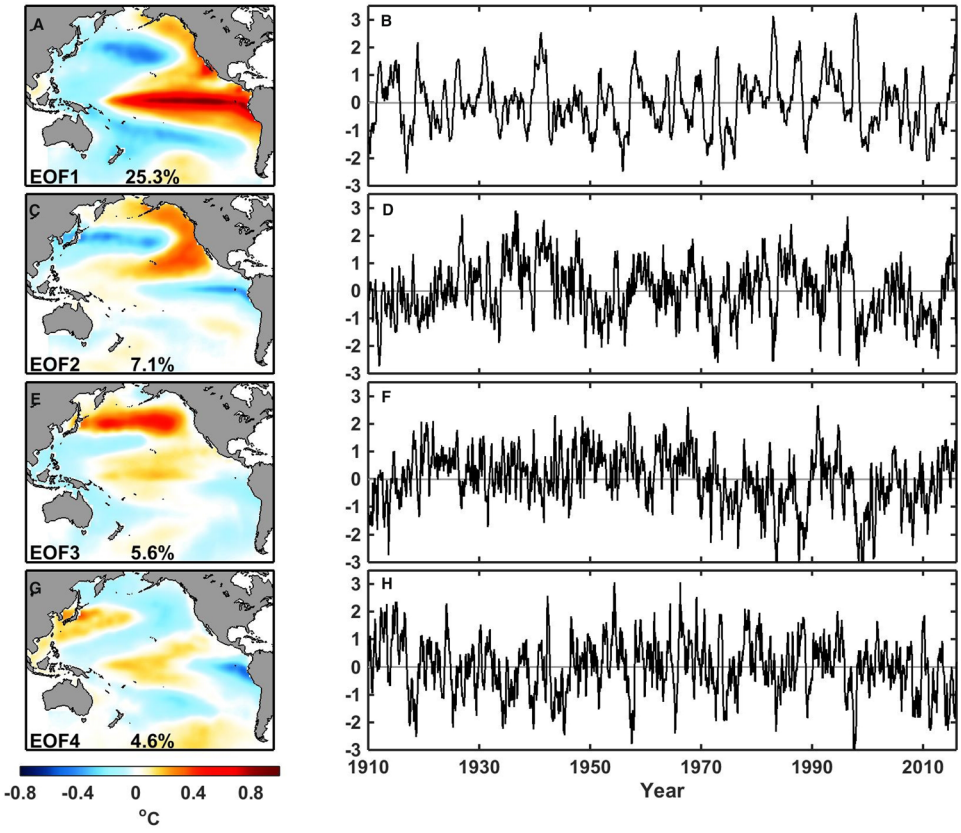

Fig. 5 First 4 conventional EOFs and their PCs of SST* in the pan-Pacific domain

variability contained in the tropical ENSO-like mode and the decadal variability associated with the extratropical PDO. This PC is often used as an ENSO index, but this practice is problematic, often leading to a biased criterion for the occurrence of ENSO that is dependent on the phase of the PDO. It is discussed in more detail by Feng and Tung (2019, submitted).

The second EOF in conventional EOF analysis is required to be orthogonal to the first while explaining the most of the remaining variance. This is formed by the difference of the leading regional modes in the two subdomains. This combination is orthogonal to the leading pan-Pacific EOF, which is the sum of the same two regional modes. Features of this combination can be seen in Fig. 5. The second pan-Pacific EOF has the approximate spatial features of the difference of the two regional leading EOFs. The bullet-like feature associated with the extratropical PDO appears in both the first and second pan-Pacific EOFs, while the sign of the tropical ENSO is reversed in the second. A combination of the two second-regional modes, the Victoria mode and the ENSO Modoki mode, would satisfy the orthogonality requirement, but its variance turns out to be less than the difference of the two leading regional modes.

The difference and sum of the second regional EOFs in the extratropical and tropical subdomains become the third and fourth EOFs in the pan-Pacific domain. These are orthogonal to first and second EOFs in the pan-Pacific domain because they are orthogonal to the latter's regional component in each subdomain. Ashok et al. (2007)'s ENSO Modoki mode is now seen to be present in both the third and fourth pan-Pacific modes, mixed in with the extratropical Victoria mode. To uncover the ENSO Modoki mode in the pan-Pacific domain, one needs to add and subtract the third and fourth pan-Pacific EOFs. This is a special case of pair-wise rotated EOF, with an angle of rotation of 45°.

3 Pair-wise rotation of PCs

Mode mixing could arise from mixing of regional modes in a larger domain, here the pan-Pacific domain, as discussed above. Or it could be a mixing of two or more centers of action in space. Or it could be a mixing in the frequency domain, where the decadal frequency band is mixed with the interannual-frequency band. Depending on what one wants to accomplish, rotation of the PCs through different angles results in different spatial patterns in the EOFs and frequency bands in their PCs.

Conventional EOF analysis requires that both EOFs be orthogonal to each other and their PCs also be orthogonal (i.e. uncorrelated) with each other. Since few large-scale physical modes can satisfy such a twin orthogonal

constraint, they are often broken into different pieces and combined mathematically into the EOFs and PCs, resulting in mode mixing.

Takahashi et al. (2011) added and subtracted two leading PCs of the regional SST* EOF analysis in 10°S–10°N, while Chen and Wallace (2016) added and subtracted two leading PCs of the pan-Pacific SST*. These operations are equivalent to 45° rotations of the PCs. These results are generalized to global SST and rotation through any angle in Chen, Wallace and Tung (2017) (hereafter CWT). A review of the literature on rotated EOF analysis can be found in CWT.

We relax the spatial orthogonality constraint of conventional EOF analysis by adopting the newly introduced procedure of pair-wise rotation of the Principal Components (PCs) (CW16 and CWT). The rotated PCs are still orthogonal and normalized but the EOFs are not necessarily orthogonal, and as such hopefully closer to the physical modes. The motivation for rotating the PCs was given by CWT: as a way to remedy the mode mixing, which arises as a mathematical artifact of the twin orthogonality constraint. Two objective criteria were proposed in CWT. Using an objective criterion of minimizing the overlap of the frequency bands [specifically, minimizing the FASC (frequency averaged squared covariance)], CWT found that the optimal angle of rotation is 43° for the leading pair of the dynamical PCs (after the trend) in the global SST expansion. In the pan-Pacific case, the optimal angle is found here to be 46°. If instead the objective criterion is to separate the centers of action spatially (by minimizing the SASC, spatially-averaged squared covariance), then the desired rotation angle is 18° in the pan-Pacific case. We could have used the 18° rotation angle, which better separates the extratropical center of action from the tropical one, but the resulting PC associated with the extratropical center of action is not well correlated with the commonly used PDO index of Mantua et al. (1997). The 46° rotation yields a decadal PC that is highly correlated with the common PDO index (at over 0.9 correlation coefficient) at the expense of the PDO extending somewhat into the central equatorial Pacific. Here, our primary purpose is to obtain pan-Pacific EOFs that have identifiable regional patterns defined by previous authors, and highly correlated with commonly used time indices associated with such regional definitions. A simple addition and subtraction of a pair of PCs are used here, following CW16 for pan-Pacific SST, which is equivalent to a 45° rotation. Visually the results are indistinguishable from the 46° rotation. Since the rotation angle used here happens to be the same as in CW16 for the purpose of removing frequency mode-mixing, the decoupling of frequency mode-mixing between the decadal frequency of the PDO and the interannual frequency of the ENSO is also accomplished in the process for the first pair of mode-mixed PCs. This bonus is not necessarily true for the higher modes in general.

For reasons specific to the procedure (see CWT), SST anomaly instead of SST* is used here for the RPCA. SST* is used above when we are comparing with previous work which used SST*. In general it is more desirable to use SST anomaly instead of SST*. SST* is SST with the global mean SST subtracted. The latter contains a large Atlantic signal because the Atlantic Multidecadal Oscillation (AMO) has been shown to strongly affect the global-mean SST (Chen and Tung 2018). The use of SST* introduces a negative AMO signal to the Pacific and reduces the amplitude of the AMO in the Atlantic. When SST is used, as done here, the trend remains in the data and may show up in all modes. The treatment of such trends will be discussed later and in the "Appendix".

The rotation of a pair of PCs through an angle θ is given by the following formula:

$$prPC_i = \cos\theta PC_i - \sin\theta PC_j$$
$$prPC_j = \sin\theta PC_i + \cos PC_j$$

The pairs: PC2 and PC3, and PC4 and PC5 are rotated here through a 45° angle. This is equivalent to adding and subtracting the two PCs involved, and then normalizing the result by dividing by the squared-root of 2:

$$prPC_i = \left(PC_i - PC_j\right) \Big/ \sqrt{2}$$
$$prPC_j = \left(PC_i + PC_j\right) \Big/ \sqrt{2}$$

prPC1 is the global warming trend mode (denoted by TR here). The dynamical modes, prPC2 and higher, have no trend, their trends have been transferred to prPC1 through a trend transfer algorithm using the above pair-wise rotation formula but with the tangent of the angle determined by the ratio of the slopes of the two PCs involved (see CWT and the "Appendix" here).

The leading four EOFs and their prPCs are shown in Fig. 6.

We find that the leading modes of variability in the pan-Pacific SST are, after the global warming trend: the canonical ENSO (called ENSO-cycle by CW16), the pan-Pacific PDO (denoted by pan-PDO here) and a third mode which we call the Central Pacific Variability (CPV) mode. The fourth mode is similar to the NPGO/Victoria mode (Di Lorenzo et al. 2008), and will be called NPGV here. The ENSO-cycle mode is tightly confined to the equator and has little extratropical variance. The PC of our pan-PDO is highly correlated with the PC of the traditionally defined PDO as the leading PC of SST* north of 20°N in the Pacific. The spatial structure of the pan-PDO mode is virtually identical to the regionally defined PDO: Its center is a cold bullet-like region in the northwest Pacific surrounded by warm SST in the northeastern Pacific. We therefore identify our REOF3/prPC3 as the pan-Pacific counterpart of the traditionally

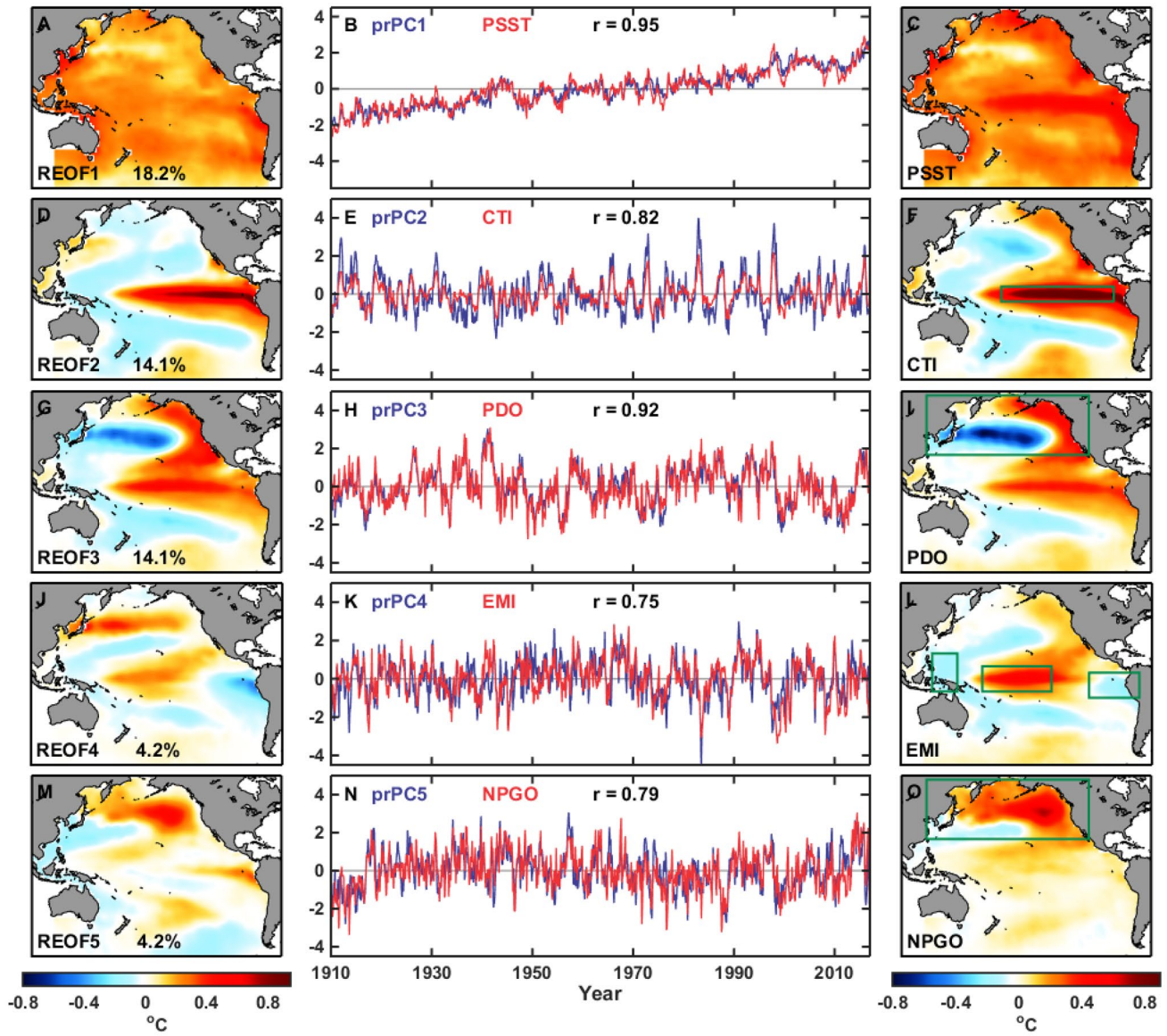

Fig. 6 Pair-wise rotated EOFs/PCs of pan-Pacific SST. The prPCs (in blue) are compared with the regional indices (in red) in the middle column, with the correlation coefficient (r) indicated; all are statistically significant at 95% confidence level. In the right column, the regions used in defining the regional indices are boxed in green. The spatial patterns in the right column beyond the green boxes are obtained by regressing pan-Pacific SST onto these regional indices

(and regionally) defined PDO. The pan-Pacific version has a weak extension of the warm SST into the central equatorial Pacific, and could represent the effect of the North Pacific PDO on the central tropical Pacific SST on decadal time scales. This extension tapers off in the eastern equatorial Pacific, diminishing its effects on the EP ENSO.

The third mode has a horseshoe shaped warm SST in the central tropical Pacific extending in an arc to the northeastern Pacific of the same sign. Feng et al. (2014) previously proposed that the warm SST off Baja California may be a trigger for the formation of CP El Niño. This third mode has an opposite signed anomaly in the eastern equatorial Pacific. Its tropical SST pattern is roughly similar in structure as the ENSO Modoki mode obtained by Ashok et al. (2007) in an EOF analysis restricted to the tropical Pacific, accounting for only 45.8% of its variance, however. This is because the older index, the MPC index, is contaminated by PDO, as discussed previously and will be shown quantitatively later. Other previous authors also obtained a roughly similar structure for their second EOF in a domain restricted to the tropical Pacific (Yeh and Kirtman 2004; Sun and Yu 2009; Choi et al. 2013). The current result simply puts it in a pan-Pacific context. The fourth mode has a significant variance in North Pacific, and has a high correlation with NPGO/

Victoria index defined by the second PC of SST* north of 25°N in the Pacific (r = 0.85). It will be called the NPGV mode here. The NPGV mode is similar to its regional counterpart. It has very little variance in the tropical Pacific and plays very little part in expressing the ENSO diversity.

EOF modes are not necessarily physical modes. Physical interpretations of ENSO and PDO modes have been discussed in literature by previous authors, based mostly on regional indices or regionally defined leading EOFs. In the second column of Fig. 6 we reproduce these regional indices and show that they are highly correlated with our rotated PCs—this is not the case with the conventional PCs. In particular our ENSO-cycle mode is very similar to model produced "ENSO-cycle" (Zhang et al. 1997), with a spatial pattern more tightly focused on the equatorial Pacific than that of the conventional EOF version. Its confinement to the equatorial Pacific in models of ENSO [see Sarachik and Cane (2010)] was explained as a result of equatorially confined Kelvin and mixed Rossby waves propagating across the equatorial Pacific waveguide. Our pan-PDO is highly correlated with the regionally defined PDO index of Mantua et al. (1997) (r = 0.92 in 3-month running mean). So it can be regarded as the pan-Pacific generalization of the regionally defined PDO, and we shall use the abbreviations pan-PDO and PDO interchangeably depending on context. These two PCs (ENSO-cycle and pan-PDO) are orthogonal (uncorrelated) in our rotated EOF analysis by virtue of the fact that their frequency ranges do not overlap. Nevertheless it does not follow that the two physical phenomena are independent. In a paper entitled "ENSO-forced variability of the Pacific Decadal Oscillation", Newman et al. (2003) showed that variability on decadal time scales of the PDO can be reproduced when tropical ENSO was introduced as a forcing term in an AR1 model. Chen and Tung (2018) repeated that model calculation and found that the oft-quoted result of ENSO generating the PDO is actually an artifact: the tropical ENSO forcing used by Newman et al. (2003) actually contains both ENSO and PDO time series in almost comparable proportions. When the ENSO-only forcing was used, the PDO that was "forced by ENSO" disappeared. These experiments suggest that the ENSO-cycle and PDO modes are likely distinct physical modes, with the PDO mode likely locally forced by air-sea interaction in the midlatitude Pacific, integrated by the slower ocean variability. We will propose a physical interpretation of the third, the CPV mode, later.

4 Expressing ENSO diversity in terms of the three leading modes of pan-Pacific SST

We shall show next that the variability in the tropical Pacific, including that in the Central Pacific, can be expressed in an orthogonal expansion involving mainly the first three modes identified above. The fourth mode is important only in the northern Pacific. This will then allow us to understand the evolution of the ENSO variability through the past 100 years. As an orthogonal space–time expansion of the SST, it is mathematically applicable whether the CP El Niño is an evolving state or a stationary pattern.

Since the SST can be expressed in an orthogonal expansion of the rotated PCs, with their coefficient being the rotated EOFs, many SST-based indices can be written as a combination of these modes:

$$SST(\mathbf{x}, t) = \sum_{j=1}^{\infty} EOF_j(\mathbf{x}) PC_j(t). \tag{1}$$

This expansion works whether the PCs are rotated or not, since both conventional and rotated PCs are orthogonal. Specializing to the leading rotated modes, we can rewrite Eq. (1) as

$$\begin{aligned} SST(\mathbf{x}, t) = {} & TR(\mathbf{x}) \cdot prPC_1(t) + ENSO(\mathbf{x}) \cdot prPC_2(t) \\ & + PDO(\mathbf{x}) \cdot prPC_3(t) + CPV(\mathbf{x}) \cdot prPC_4(t) \\ & + NPGV(\mathbf{x}) \cdot prPC_5(t) + \cdots \end{aligned} \tag{2}$$

In Eq. (2), the dependence on latitude and longitude is abbreviated as **x**, and short-hand notations are used for the rotated EOFs. For example the spatial pattern associated with $prPC_2$ is denoted by ENSO(x). Here we list the definition of various ENSO indices, such as Niño 1 + 2, Niño 3, Niño 4, Niño 3.4 etc. in Table 1 [Rayner et al. 2003; Mega-ENSO from Wang et al. (2013); JMA from http://ds.data.jma.go.jp/tcc/tcc/products/elNiño/]. The most commonly used region is the Niño 3.4 region, because this region encompasses the western half of the equatorial cold tongue and the Central Pacific, and provides a good measure of important changes in SST and SST gradients that result in changes in the pattern of deep tropical convection and atmospheric circulation. Other indices that are different from typical ENSO indices have also been proposed for studying ENSO diversity. For example, the Trans Niño Index (TNI) that was proposed by Trenberth and Stepaniak (2001) is defined as the difference of normalized SST between Niño 1 + 2 and Niño 4 indices. This index measures the east–west temperature gradient in the tropical Pacific and can indicate the evolution of ENSO events. The ENSO Modoki Index (EMI) is constructed as the difference of SST averaged over the Central Pacific, and over western and eastern Pacific. It was used to distinguish a new type of ENSO event, namely CP El Niño. Different from area-averaged SST, the MPC index is given by the second PC of Tropical Pacific SST. The MPC has a high correlation with EMI index, also reflecting the variation of the Central Pacific and ENSO diversity.

Figure 7 shows in bar charts the contribution to each ENSO index by the fundamental modes in percentage

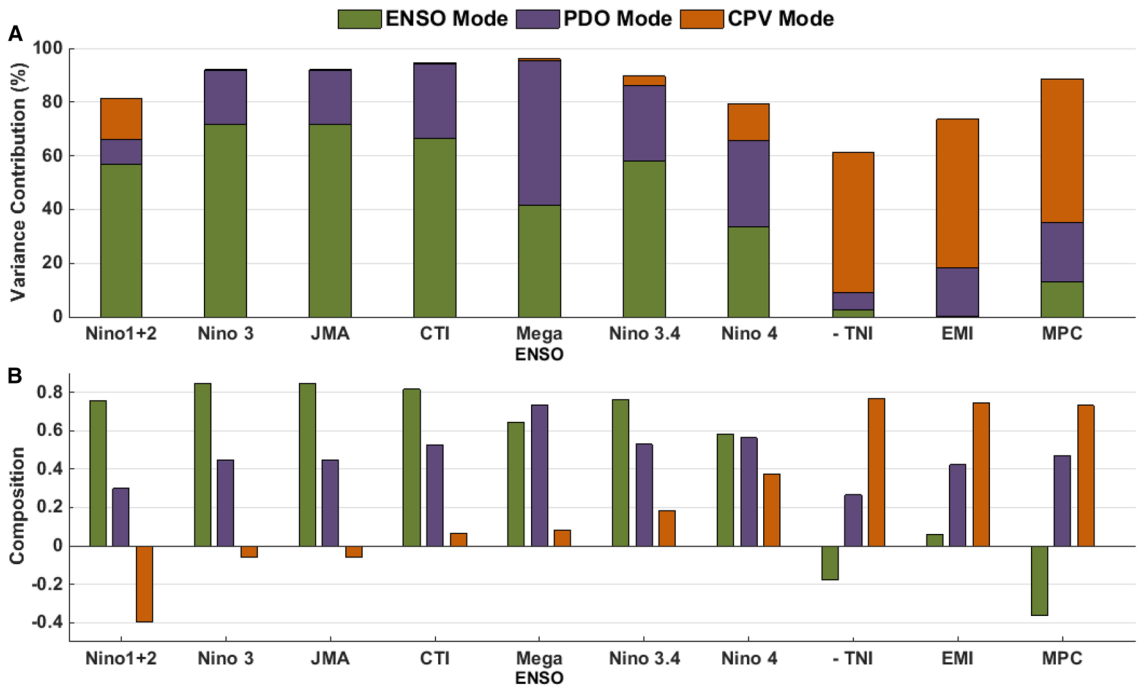

Fig. 7 Contribution to each ENSO index by the fundamental modes, in percentage of variance (top panel) and as each index' composition (bottom panel). The composition to each ENSO index is obtained by the expansion coefficients of the SST involved in the definition of the index. The indices have been detrended

variances explained (top panel). Conventional ENSO indices can be mostly expressed by two modes, the ENSO-cycle mode and the pan-PDO mode. The CPV mode plays a more important role in indices involving CP ENSO and ENSO diversity, like TNI, EMI and MPC index, accounting for about 50% of the each of their total variance, while the ENSO-cycle mode has smaller contributions to the CP ENSO phenomenon. The sum of the three fundamental modes (ENSO-cycle, CPV and pan-PDO) explains close to 80% of the variances of most of the indices, except for an index that is defined as differences of normalized SST (viz. TNI at 60% variances explained by the three modes) instead of normalized difference of SSTs. The combination of different normalizations alters the SST structure from the original SST used to derive the EOFs. The NPGV mode has negligible contribution to all tropical ENSO indices. The TR mode is only necessary if the ENSO indices have not been detrended.

For some ENSO indices, the contribution by the CPV mode is negative, as shown in the bottom panel of Fig. 7. For the Niño 1 + 2 index, which measures the easternmost Pacific SST in the equatorial region, an increasing amplitude of CPV reduces the occurrence of EP El Niño, while negative CPV adds to the amplitude of EP El Niño. It turns out that for extreme EP El Niño events, such as the 1982–1983 and 1997–1998 events, a negative CPV is associated with a deepened thermocline reaching all the way to the easternmost Pacific. On the other hand, positive CPV contributes positively to the Niño 4 index, which measures the SST in the Central Pacific, implying that it increases the likelihood of occurrence of CP El Niño, since one of the criteria for classifying an event as CP El Niño is that its Niño 4 SST is warmer than its Niño 3 SST, even if only slightly (Yu et al. 2012). Consistent with that, the CPV mode significantly increases in the positive direction the main CP El Niño indices: EMI, MPC, and -TNI. (Negative TNI is Niño 4 minus Niño 1 + 2; see Table 1). In fact, one can see that these indices are increased by the in-phase portion of PDO and the CPV modes, with the CPV mode providing the most contribution.

Although the variance of the pan-PDO is three times that of the CPV mode, most of its variance is centered in the North Pacific. In the central equatorial Pacific, the variance of the two modes is comparable. Of the indices commonly used to measure the CP ENSO, the EMI and MPC, the contribution by the CPV mode is actually slightly larger. Figure 7 bottom panel shows that when pan-PDO and CPV are in phase, CP El Niño is more likely to occur, as measured by the EMI and MPC indices.

5 Changes in the CPV mode before and after 1970s

As we mentioned above, the CPV mode accounts for about half of the variation of ENSO Modoki indices. We also find that this mode has a low-frequency behavior that is different

before and after about 1970. We perform RCPA separately for the period before 1970 and after. Figure 8 shows the result: the Central Pacific variance of this mode strengthened after 1970. Its variance increased by four times in the 1980s and 1990s. It declined since 2000, perhaps in response to the global warming slowdown (see later), but nevertheless the variance in the 2000s is still twice that prior to 1970s. We refrain from commenting on its variance prior to 1950s as there may be concerns about the quality of data in the earlier period.

6 Tropical trade wind intensification

The trade winds in the tropical Pacific, which could play an important role in determining whether an El Niño's maximum SST occurs in the eastern or Central Pacific, has strengthened since 1970s. Figure 9 shows the linear trend of the trade wind stress. It indicates that the trade winds are increasingly more easterly. It induces a SST anomaly trend that is negative in the eastern half and positive in

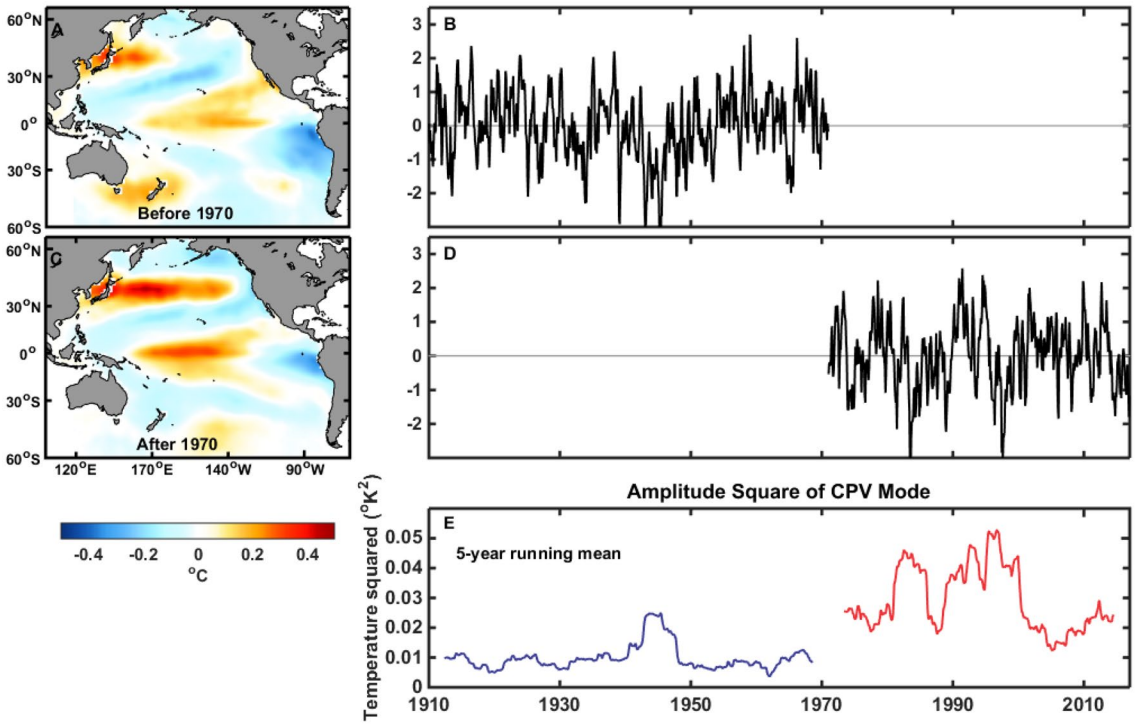

Fig. 8 Separate EOF analysis for the period before 1970 and the period after 1970, showing the increase in amplitude of the horseshoe warm region after 1970. **B**, **D** are the normalized PC. **A**, **C** their corresponding EOF in degrees K. **E** is the variance obtained by taking the square of the normalized PCs and multiplying them by the respective EOF amplitude squared in the central equatorial Pacific inside the green rectangle in Fig. 6L

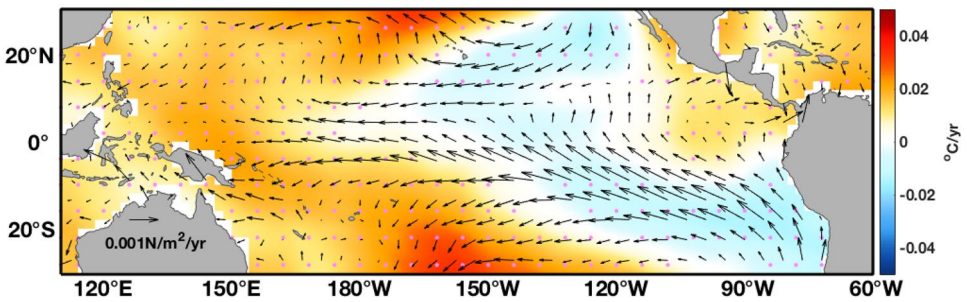

Fig. 9 Multi-decadal trends of trade winds and SST: Observed 1979–2015 linear trends in surface wind stress (N m^{-2} $year^{-1}$) shown as vectors; only those vectors with at least one component exceeding 95% confidence level are plotted. The observed trends in sea-surface temperature are overlaid in color (°C $year^{-1}$), also for 1979–2015. The regions with SST trends above 95% confidence level are shown with pink dots. The SST trend pattern, which is La Niña-like, is robust for the past 4 decades with respect to 15-, 20-, 30-, and 37-year trends

the western half of the tropical Pacific, an increasingly La Niña-like mean state.

It appears that it is the direction of the increasing northeasterly wind anomalies north of the equator and the increasing southeasterly wind anomalies south of the equator in the eastern Pacific that are producing the horseshoe pattern of SST, resembling the one in the CPV mode in Fig. 6. We shall discuss later the effect of trade winds on the equatorial thermocline and SST.

A similar figure on trade wind and SST trends since 1980s was previously shown by Hu and Fedorov (2018), with additional information on precipitation trends. Hu and Fedorov (2018) emphasized the role of the cross-equatorial component of the winds in keeping the Inter-tropical Convection Zone (ITCZ) to the north of the equator and in reducing ENSO variability in the eastern Pacific in recent decade. Here we shall focus on the longitudinal component of the trade wind intensification.

7 Mechanisms

7.1 Previously proposed mechanisms

A more comprehensive review can be found in the review article of Capotondi et al. (2015), and in Fedorov et al. (2015). Here we highlight a few previous proposed mechanisms for the purpose of putting our current proposal in the context of prior work.

Some authors view the existence of two types of El Niño as due to the decadal modulation of ENSO amplitude (e.g., Yeh and Kirtman 2004; Rodgers et al. 2004; Sun and Yu 2009; Choi et al. 2012, 2013). Sun and Yu (2009) found that there is a nonlinear amplitude modulation of the ENSO, as measured by the Niño 3.4 or Niño 3 index. In decades when the ENSO index is strong, EP El Niño is more likely to occur, while the La Niña is more likely to occur in the Central Pacific. When it is weak, CP El Niño is more likely, and the La Niña is more likely to occur in the eastern Pacific. We shall re-interpret this result later as: In the presence of the Pacific trade wind intensification in the recent decades, the thermocline is shallower in eastern equatorial Pacific, and its SST is colder. El Niño is often stalled in the Central Pacific and becomes weaker. The colder SST in the eastern Pacific favors the formation of La Niña. The asymmetry between El Niño and La Niña is consistent with the strength of the prevailing easterly trade winds, which the former must overcome. La Niña on the other hand is cold in the eastern equatorial Pacific, and is favored by the intensified trade winds.

It is also thought that the mean state of the tropical Pacific plays a role in different ENSO types initiated by westerly wind burst (or bursts). If the tropical Pacific upper-ocean heat content is larger than normal, a condition referred to as a "recharged" state, in numerical experiments westerly wind bursts can lead to an EP El Niño (Lengaigne et al. 2004); otherwise a "neutral" or "discharged" mean state will lead to a CP El Niño event (Fedorov et al. 2015). In the absence of the westerly wind bursts, a recharged state will develop into a CP El Niño within a year. We will discuss later the role of westerly wind bursts in the observed record.

7.2 Mechanism involving trade winds and thermocline depths

We have shown in Sect. 6 that the trade wind intensification is associated with an increasingly La Niña-like basic state, favoring the westward shift of the maximum warming of El Niño events. Here we study the effect of the CPV mode on the thermocline depth. The main thermocline in the tropical Pacific is commonly defined by the 20 °C isotherm. The climatological thermocline depth slopes up steeply in the eastern equatorial Pacific. When the easterly trade wind in the Central Pacific strengthens, it raises the thermocline depth in the eastern Pacific. The advection of the warm water in the mixed layer (above the thermocline) towards the west deepens the thermocline in the Central Pacific even more. On top of the secular trend, interannual fluctuations in the trade wind also increased (see later). Because of the shallower thermocline in the eastern Pacific, thermocline changes there are more obvious and this region is more sensitive to trade wind variations. This correlation holds for the trend as well as for their interannual variations. The latter is shown in Fig. 10. The highest correlation is between the surface zonal wind stress anomaly (negative trade wind stress anomaly) in the Central Pacific (i.e. Niño 4 region) and the thermocline depth in the Eastern Pacific (i.e. Niño 3 region), for the reason given above. The correlation coefficient is 0.58, which is statistically significant at 99% confidence level (top panel), even taking into account the effect of autocorrelation in reducing the degree of freedom (Ding et al. 2012). The correlation is even higher if we consider only boreal winters (lower panel). The correlation coefficient is 0.87, at 99% confidence level.

Figure 10 also shows what is commonly known. During an El Niño event, the easterly trade wind weakens and the thermocline slope is flattened (and therefore deepened in the Niño 3 region) as the warm mixed-layer water sloshes to the eastern Pacific.

A positive CPV tends to create an opposite pattern of raised thermocline in the east and deepened thermocline in the Central Pacific. Such an anomaly is sometimes overcome by a strong ENSO-cycle mode, leading to an EP El Niño event. In other times, a strong CPV and moderate or weak ENSO-cycle then stall the El Niño in the Central Pacific. Figure 11C shows that the difference between the ensemble-mean of CP El Niño events and that of the EP El Niño in

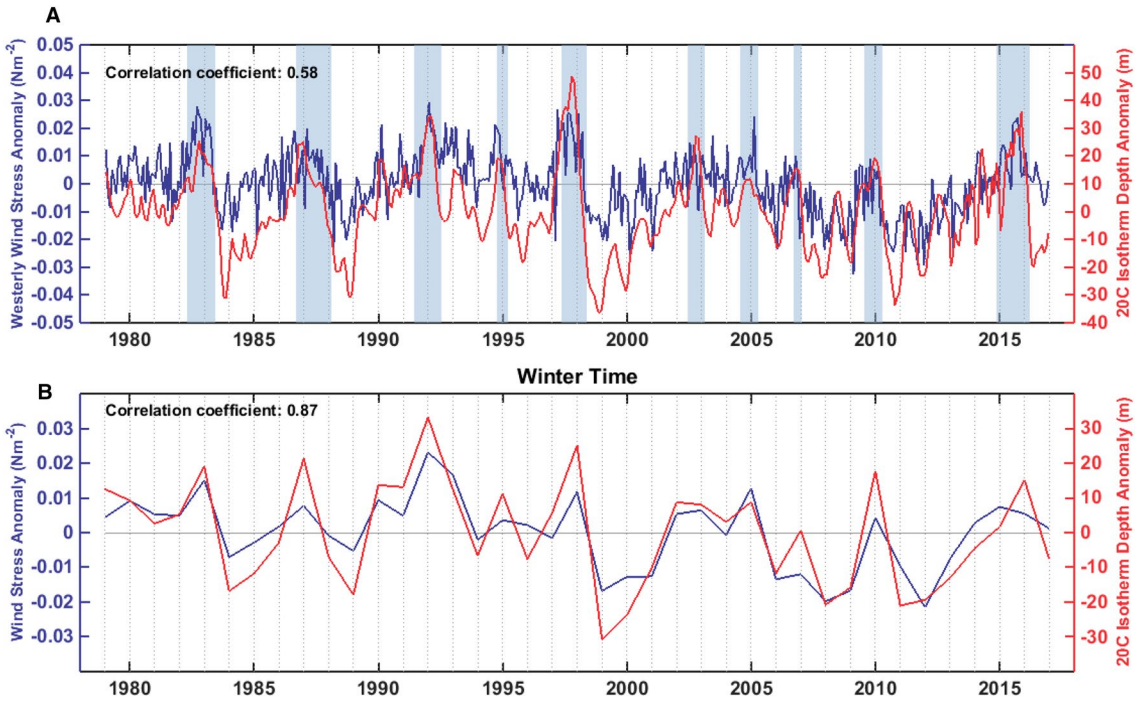

Fig. 10 Time series of zonal surface wind stress anomaly averaged over the Niño 4 region of the tropical Pacific and the 20 °C thermocline depth anomaly averaged in the Niño 3 region (monthly in the top panel and boreal winter months in the lower panel). The vertical light blue shades indicate the duration of El Niño events. The subsurface data are from Ishii (Ishii et al. 2005, 2006; Ishii and Kimoto 2009); 2012 is the last year that they are available. We merge them with Argo data available for 2004–2016

color, with the individual cases taken from Fig. 11A, B. Compared to EP El Niño, CP El Niño deepens the thermocline in the Central Pacific while making it shallower (in comparison to the deepening by the EP El Niño) in the Eastern Pacific. As shown previously in Fig. 7, CP El Niño indices are dominated by the changes in CPV and pan-PDO (abbreviated as PDO in the figure) mode, while the EP El Niño, being the canonical ENSO, is dominated by changes in our ENSO-cycle fundamental mode (abbreviated as ENSO in the figure). So the difference of the two types of El Niño should be explained by (CPV + PDO)-ENSO. This quantity is then superimposed onto the actual historical difference in the thermocline depth between the two types of El Niño events, with the magnitude of each of the fundamental modes obtained by regressing the thermocline variation for each event onto the fundamental modes. The agreement is remarkable, not only in the spatial distribution but surprisingly also in amplitude.

8 El Niño evolution

Despite the rising trend of trade winds in the mean state, there are instances when they temporarily weaken on monthly timescales. Figure 12 shows that every El Niño event is preceded by one or more westerly wind bursts (WWBs) in the Central Pacific before the boreal winter, creating a comparable deep minimum in the easterly wind, despite a generally intensifying trade wind: It is interesting to note that prior to the strong EP El Niño events, the minimum value of the easterly wind reached in the Central Pacific is deep and almost the same even though the general trend of the easterly wind is rising in other seasons. The WWB strength, as measured by easterly wind stress anomaly (not shown) is strongest prior to the occurrence of extreme El Niños, in 1982–1983, 1997–1998 and 2015–2016, as compared to other El Niño events.

One reason for the increased interannual variability was given by Eisenman et al. (2005): WWBs are more likely when the warm pool is extended more eastward, as in the case with strengthened trade winds, which move warm surface water from the eastern to the Central Pacific. The westerly wind burst that preceded the CP El Niño is weaker, as previously pointed out by Xiang et al. (2013).

The lower part of Fig. 12 shows that during (not prior) the time of an El Niño event, the easterly wind in the eastern Pacific attains a moderate maximum. This is due to the two-cell circulation generated by the convection over the warm SST in the Central Pacific in an evolving El Niño: the returning flow to the east of the convection is easterly [see Sarachik and Cane (2010)]. This easterly surface wind stress stalls the eastward movement of some of the moderate and

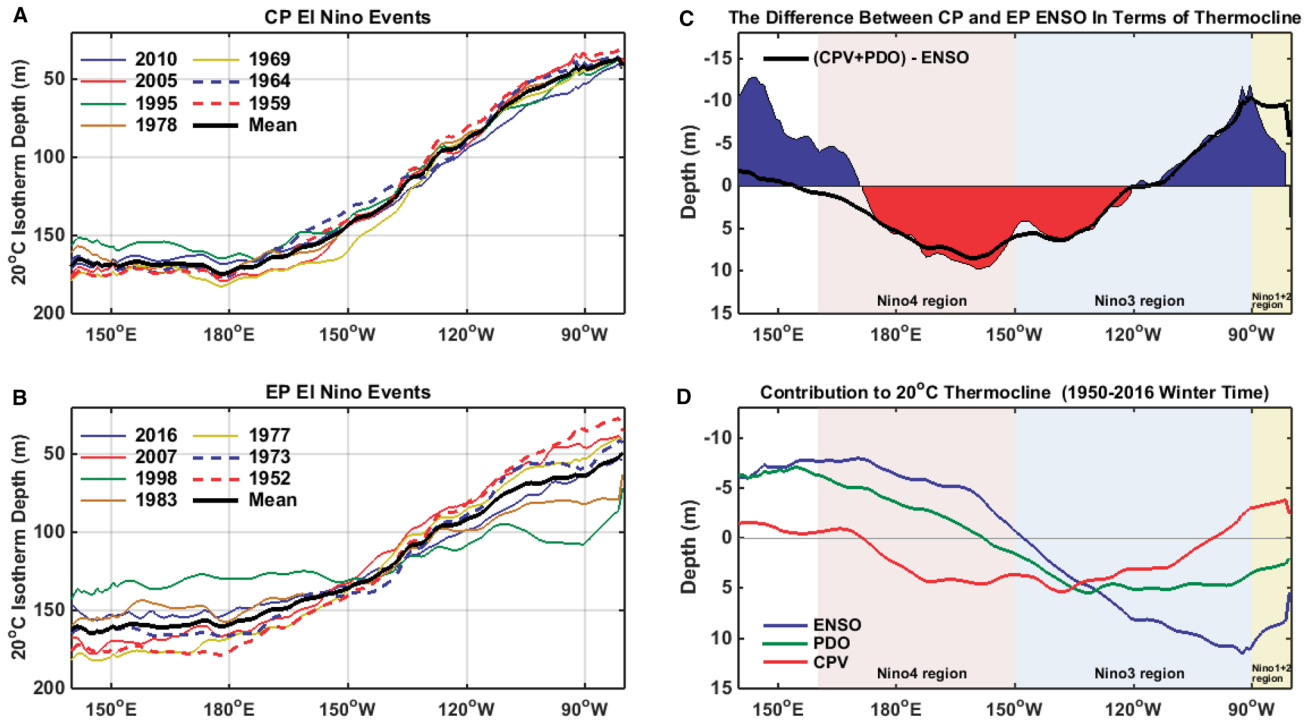

Fig. 11 Thermocline depth for typical CP and EP El Niño events and the difference between them. Thermocline depth as defined by the 20 °C isotherm in the equatorial Pacific (averaged over 2°S–2°N) for 1950–2016, as a function of longitude. Five-month boreal winter means are used. The individual CP El Niño events (A) and EP El Niño events (B) are chosen based on the classification of Yu et al. (2012) as consensus of three criteria. The dark curve in **A** and **B** is the ensemble mean of the seven cases for each type. The difference in the equatorial thermocline depth between the CP El Niño and EP El Niño (**C**) is shown in color. Red denotes depth deeper than the basin mean and blue shallower than the basin mean. **D** Represents the regression of the 5-month boreal winter mean equatorial thermocline depth onto each of the three fundamental modes at each longitude. The difference of the CP and EP El Niño can be explained by (CPV + PDO)-ENSO, shown superimposed in (**C**), with the magnitude of each of the fundamental modes determined from the regression shown in (**D**)

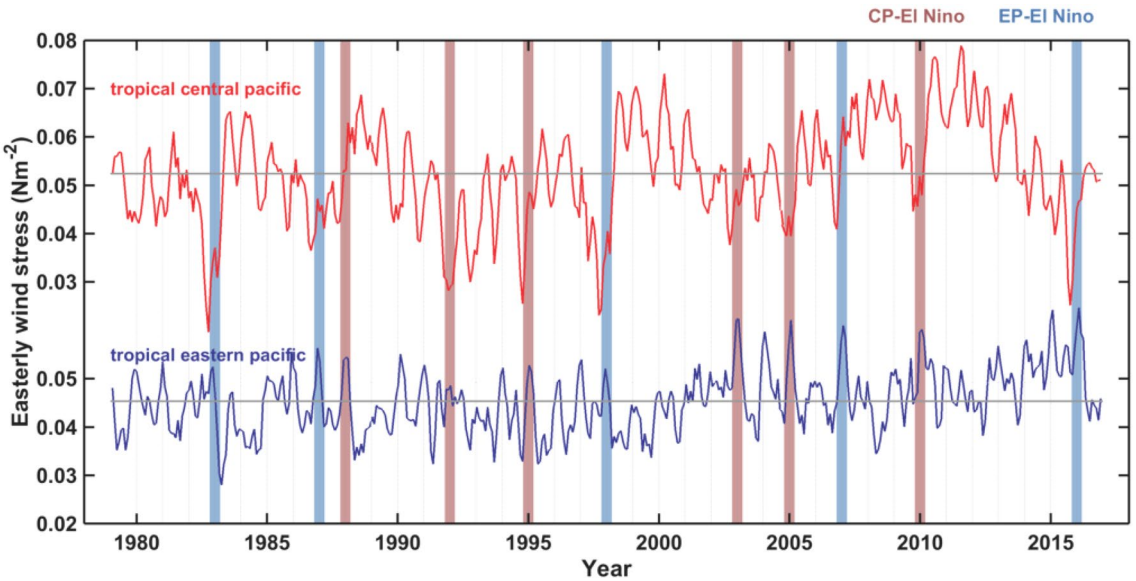

Fig. 12 The tropical easterly wind stress in different regions. The red curve denotes the wind stress in Central Pacific (zonal averaged over Niño 4 region). The blue curve indicates the change of wind stress in eastern Pacific (zonal averaged over 240°E–260°E). The vertical lines indicate the occurrence of EP El Niño (in blue) and CP El Niño (in maroon)

weak El Niños, forming the "standing CP Warming" referred to by Xiang et al. (2013). For the very strong El Niños, the initial strong WWBs and the associated oceanic flow to the east are able to overcome this easterly wind resistance to reach the easternmost Pacific. Then the cell to the east is no longer over the ocean, and the warm SST associated with the El Niño reduces or even reverses the SST zonal gradient. The Bjerknes feedback maintains the surface wind stress to be consistent with the SST gradient over the roughly 1-year duration of the event (see Fig. 10).

Capotondi et al. (2015) additionally mentioned that 6 months prior to the final state of the EP El Niños, a warm SST first appears in the far eastern Pacific during spring. This could be the oceanic manifestation of the relaxation of the trade wind in the Central Pacific mentioned earlier. WWBs in the Central Pacific send an oceanic Kelvin wave to the east, depressing the thermocline and creating a positive SST anomaly in the Eastern Pacific (Capotondi et al. 2015). This is a part of the evolution of EP Niño.

9 Extratropical influence of CP El Niño

Pan-PDO and CPV modes are likely to be both in phase and positive during the boreal winter for the occurrence of CP El Niño events. This may be interpreted as extratropical influence of the CP El Niño phenomenon. However, is a positive phase of pan-PDO actually necessary for the occurrence of CP El Niño? One way to find out is to examine a period when decadal variation of the PDO is negative. However the observed record for CP El Niño is short, and the decadal PDO is mostly positive during this period. Alternatively, since the SST can be decomposed into the fundamental modes, we can delete the contribution of the PDO, reconstruct the SST and then decide if the CP El Niño events can still occur according to the established criteria.

Figure 13 top panel shows the boreal winter averaged SST field during the CP El Niño events; the years are chosen according to Yu et al. (2012) as consensus of three criteria. The reconstructed SST field after the pan-PDO

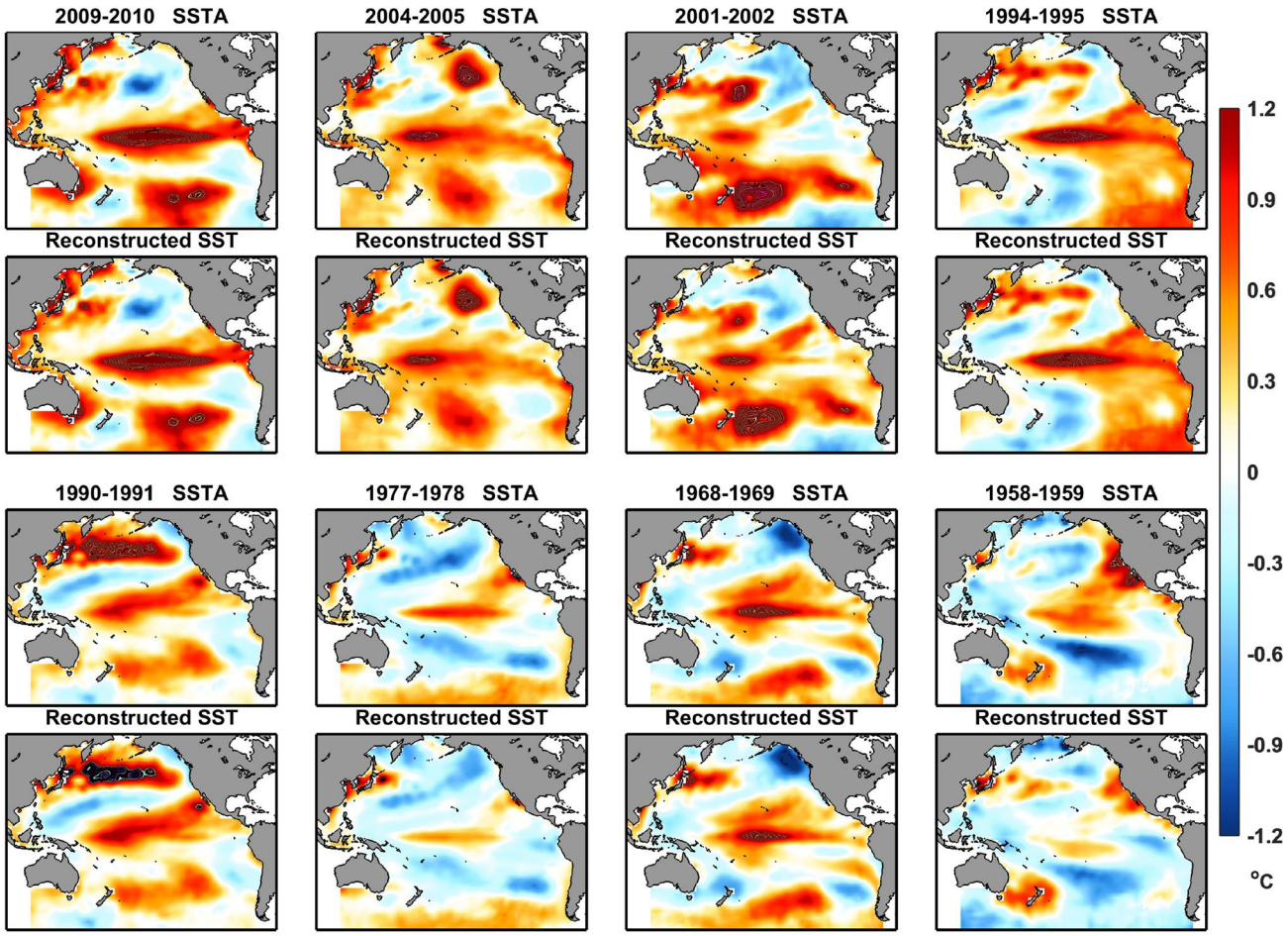

Fig. 13 SST in the Pacific during the years of CP El Niño, averaged over the boreal winter (top row), and reconstructed SST after the pan-Pacific PDO's contribution to the SST has been deleted (bottom row)

contribution is regressed out from the SST is shown in the lower panel. The criterion most sensitive to the PDO contribution is the one that requires the SST in the Niño 4 region be higher than that in the Niño 3 region. This criterion is still satisfied even after the pan-PDO contribution is removed. One qualification: the definition of an El Niño event by NOAA is based by the Ocean Niño Index (ONI) index, which is the 3-month mean of Niño 3.4 index, exceeding 0.5 °C for 5 consecutive months. Since the pan-PDO affects the Niño 3.4 index (see Fig. 7), deleting the pan-PDO may render some of the weaker El Niño events to be below that threshold in the reconstructed SST: namely the 1977–1978, and the 1958–1959 events. This subjective selection criterion is however not mechanism dependent.

Therefore we conclude that the pan-PDO's influence on the occurrence of CP El Niño is not important. It is there in the observed composition of this phenomenon and in its observed ensemble averaged tilt of the main equatorial thermocline because the period of observation coincides with a mostly positive decadal PDO phase after 1979. The emergence of the CP El Niño phenomenon is likely due to the intensification of the trade winds and its effect on the CPV mode.

10 Detailed examination of individual occurrences

In Fig. 14 we show compactly the evolution of the equatorial 20 °C thermocline and the three fundamental modes of SST in a Hovmoller diagram from 1950 to 2016. We mark the time of occurrence of EP and CP El Niño events using green and maroon arrows, respectively. Classification is based on Yu et al. (2012)'s Majority (2 out of 3) rule for both CP and EP classification, and therefore contains more potential CP cases than the consensus shown in Fig. 4.

Maximum thermocline depths occur in the Central Pacific in between El Niño events and become shallower during the events. That is, El Niño events, whether EP or CP, raise Central Pacific thermocline (and deepen it to the east). The extent of the flattening to the east seems comparable between CP El Niño and moderate EP El Niño. Therefor in terms of only thermocline perturbation, CP El Niño and moderate EP El Niños are not clearly distinguishable. Strong (sometimes called "extreme") EP El Niño events, however, are characterized by their thermocline flattening all the way to the eastern coast, and their SST having a very large ENSO-cycle component and a negative CPV component; the latter helps the deepening of the thermocline in the Niño 1 + 2 region.

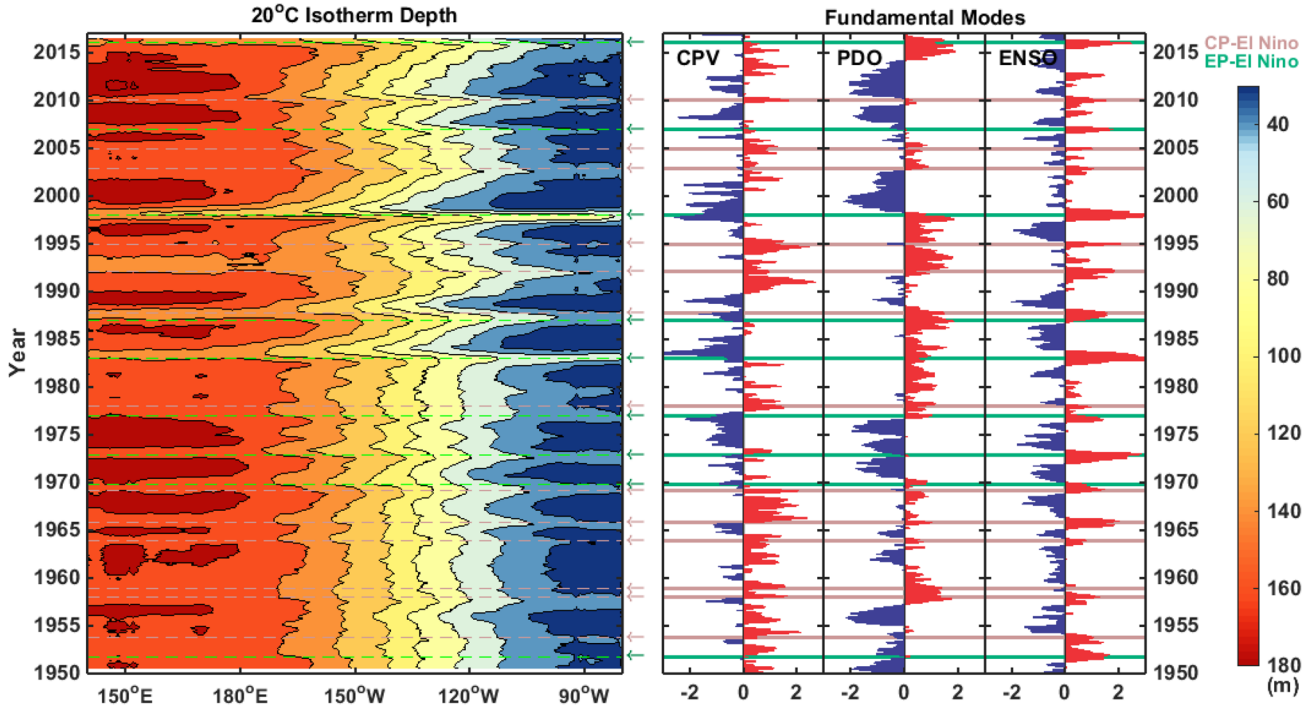

Fig. 14 Hovmoller diagrams of 13-month running mean 20 °C isotherm depth, averaged over 2°S–2°N, across the tropical Pacific (left panel); And time series of three fundamental modes of SST anomaly after 3-month running mean: ENSO mode, PDO mode and CPV mode. The occurrences of EP El Niño events are indicated by green lines, and maroon lines for the CP El Niño. Majority rule (2 out of 3) is used for deciding whether it is CP or EP El Niño

The strength of the EP El Niño, as seen by the extent and depth of the thermocline flattening, depends on the magnitude of its ENSO-cycle component of the SST decomposition. This argues in favor of using the ENSO-cycle PC as an index for EP ENSO. CP El Niño events are seen to have CPV mode being positive, and their thermocline flattening stalled, therefore not reaching the eastern Pacific. Pan-PDO component is positive during the months of the CP El Niño but, as we argued previously, the event could still be classified as CP even if PDO influence is regressed out.

There are a couple minor exceptions to the general rule mentioned above, with slightly negative CPV for CP El Niño. These are cases that do not have a consensus classification in Yu et al. (2012).

After a period of rapid warming in the 1980s and 1990s, the global warming slowed after the El Niño of 1997–1998, when we also see the beginning of the decline in the CPV amplitude in the SST in Fig. 8e. Due to the large interannual variations caused by El Niño events, the trend in the trade winds and in eastern Pacific thermocline depth are generally difficult to detect and to show significance. Nevertheless, one can see that the thermocline depth in the Niño 3 region is generally shallower in between El Niño events in the decades after 1980 than the decades before in Fig. 14 (see the light blue and yellow contours), with the possible exception of the recent decade. One can see that after the extreme El Niño event of 1997–1998, the thermocline depth in the Niño 3 region begins to deepen (corresponding to the global warming slowdown starting that time). Then the deepening is interrupted by the strong CP El Niño of 2010. After 2010, the deepening resumes until the extreme El Niño event of 2015–2016.

11 Summary discussion

A main result of the present paper is the distillation of the myriad of ENSO diversity indices first into three (ENSO-cycle, pan-PDO and CPV), and then into two fundamental modes, when we found that while PDO is present in the period of analysis it is not important in the mechanism responsible for the two type of ENSO events. With only two important parameters, all El Niño occurrences can be plotted compactly in a 2D plot of the CPV PC versus ENSO-cycle PC. This is shown in Fig. 4. CP El Niño events have positive CPV values and cluster in the region above CPV PC > 0.5, while EP El Niño events are below this threshold, generally along the ENSO-cycle PC. Currently there are at least three criteria for classifying CP El Niño and often they do not agree. When they agree all events follow the separation shown in Fig. 4. Therefore we have found that the technical problems related to the previous definition of CP El Niño can be overcome and that a single index separates CP from EP El Niño. Our new CPV mode should be used for defining CP El Niño, and our ENSO-cycle mode should be used for defining EP El Niño. The problems related to the traditional use of the Cold-tongue index or Niño 3.4 index in defining canonical ENSO are discussed in Feng and Tung (2019, submitted).

The first part of the paper is a general development of the fundamental modes expressing pan-Pacific SST variability. We find that it is necessary to increase the number of fundamental modes beyond ENSO and PDO, given the diversity of phenomena that has been discovered in recent decades. Nevertheless, only four fundamental modes are needed, with the addition of a CPV mode (with maximum variance in the central tropical Pacific) and a NPGV mode (with maximum variance in the Northeastern Pacific). Rotated EOF analysis is used to obtain pan-Pacific modes that bear the most resemblance to the regional modes in the previous definitions, and these appear to represent physical modes. In conventional EOF analysis, the regional modes are mixed in various pieces and combinations, making identification of the pan-Pacific modes difficult.

In the second part of the paper, we apply this new orthogonal expansion of Pacific SST to express the myriad of ENSO diversity indices, and find that this "diversity" of ENSO indices can be distilled to various combinations of only three fundamental modes: ENSO-cycle, pan-PDO and CPV. Of the three, the recent reported appearance of the ENSO diversity can be accounted for by changes in two modes, the pan-PDO and CPV. The CPV mode has a secular change in amplitude since 1970s, caused possibly by the observed intensification of Pacific trade winds, while the pan-PDO mode goes through its normal phase shift every few decades. Central Pacific El Niño events increase when they are positive and in phase (during the months of the event, which can occur even during a decadal negative phase of PDO).

The mean difference of the two types of El Niño in their thermocline depth variation in the equatorial Pacific can be entirely explained by (CPV + PDO) minus ENSO-cycle, with the magnitude of each component determined by regression of the thermocline variation onto the three fundamental modes. This supports our proposed mechanism through the thermocline variation in response to trade wind intensification, not only in tendency but actually adequate in magnitude. This result can be viewed in two ways: First, the CPV mode, by making the thermocline steeper towards the east, tends to stall moderate El Niño events in the Central Pacific, favoring the formation of CP El Niño. Second, as easterly trade wind intensifies in recent decades, it tilts the equatorial thermocline, making it shallower in the east and deeper in the Central Pacific, it creates an anomaly in the thermocline that is reflected in the SST that is warmer in the Central Pacific and colder in the Eastern Pacific. This

is projected onto a SST spatial pattern that is described by the CPV model. This explains the recent appearance of the CPV mode and increased occurrence of CP El Niño events.

There is currently a debate on whether there is a continuum of ENSO types or two distinct "species" of ENSO. Johnson (2013) viewed the ENSO types as a continuum, but given the finite length of observational records, a maximum of 9 spatial patterns can be statistically distinguishable: 3 moderate to strong La Niña-like patterns, 2 weak La Niña-like patterns, 2 weak CP El Niño-like patterns, a moderate CP/EP El Niño-like mixed patterns, and a strong EP El Niño-like pattern. We have shown here that the tropical SST variability can be adequately described by only three fundamental modes. It then follows that these 9 types ENSO are simply different combinations of the three modes, and only two are mechanistically important: ENSO-cycle mode in describing EP ENSO, and CPV > 0.5 in distinguishing CP El Niño from EP El Niño, as displayed in Fig. 4. Nevertheless, in terms of the location of the maximum SST during an El Niño event, given the shortness of observational record, the null hypothesis that the location can be described by a random distribution about 140°W cannot be rejected (Giese and Ray 2011).

Is the CP ENSO a new type of ENSO? To the extent that its formation depends on the CPV mode being significant, and that the CPV mode is weak before 1970s and almost nonexistent before 1950s, this phenomenon can be considered new. Caution should be raised however concerning data quality of the early period. Although the same CPV EOF shape can also be found (but with a much reduced amplitude) if the EOF analysis is performed using only data prior to 1970 (shown in Fig. 8A), it could possibly be a result of the way the early sparse data were interpolated using EOFs of the more recent data. The newly intensified CPV pattern at least since 1970s (Fig. 8C) is likely the result of the intensification of the tropical Pacific trade winds in recent several decades, which may have started in the 1950s but its trend became statistically significant only since late 1970s. The mechanism is through the effect of the easterly trade winds on the equatorial thermocline depth, with the two shown to be highly correlated. When the CPV mode is positive, the 20 °C thermocline is deeper in the Central Pacific and shallower in the Eastern Pacific, favoring the formation of CP El Niño, while weakening the EP El Niño, but not prohibiting its formation.

Yeh et al. (2009) found that for the period 1854–2007, the frequency of occurrence of CP El Niño increased 29-fold from 0.01 per year before 1990 to 0.29 per year after 1990. Yeh et al. (2009) examined CMIP3 model results and found that under anthropogenic warming the predicted weakened trade winds will flatten the thermocline under the equatorial Pacific, leading to its shoaling in the Central Pacific. It was argued that the frequency of occurrence of the Central Pacific El Niño would increase. Lee and McPhaden (2010) found an almost doubling of the intensity of CP El Niño in the observation from 1982 to 2010, and pointed out that the intensity increase could not be explained by the shoaling of the thermocline in the Central Pacific. The observed subsurface temperature showed a steepening of the tilt of the equatorial thermocline for the past 3 decades (see also Xiang et al. 2013). It created a tendency for a colder eastern tropical Pacific SST, which was observed (McPhaden et al. 2011; Xiang et al. 2013). The colder SST is a result of the observed intensification of the trade winds since 1979, which was also observed in the mean state (see Fig. 9).

The strong easterly trade winds may have stalled some but not all El Niño in the Central Pacific. The 2015–2016 El Niño still formed in the eastern Pacific, although the predicted 2014 "super El Niño" did not materialize. Because of the much stronger intensity of EP El Niño compared to the CP El Niño, a few displaced and weakened El Niño of the former kind would make a significant impact on the increase of the latter kind of El Niño in both its historical frequency and intensity. The CP El Niño of 2009–2010, which is very strong by the standard of CP El Niño, is only half as strong as that of the usual EP El Niño, and could very well be a failed moderate EP El Niño, stalled in the Central Pacific Niño 4 region. This fact is also consistent with Fig. 4: CP El Niño events contain moderate ENSO-cycle components and can be viewed as moderate El Niño stalled in the Central Pacific. The location where the stalling occurred could be a continuum, as found by (Giese and Ray 2011).

The trade wind intensification was predicted by Cane et al. (1997) as arising from anthropogenic warming. The mechanism is the "ocean thermostat" of Clement et al. (1996): a Pacific-wide heating preferentially warms the western Pacific as the eastern Pacific is maintained cold by its proximity to the shallow thermocline there. Increased convection in the west strengthened the Walker circulation, whose return flow is the trade wind. This issue is hotly debated as the CMIP models seem to be predicting the opposite tendency (see Vecchi et al. 2006), with the notable example of the GFDL ESM2M model (see Kohyama et al. 2017). England et al. (2014) thought that the observed trade-wind anomaly was caused by an internal variability called the Interdecadal Pacific Oscillation (IPO), but noted in their Supplementary Information that the IPO did not intensify as the trade winds did, as was also pointed out by Han et al. (2014). When the IPO influence was removed by a regression procedure a substantial trade-wind trend remained (England et al. 2014). In observation since 1979, the trade winds have intensified through both positive and negative phases of the IPO. This argues against the IPO as a cause of the multi-decade long intensification in the Pacific. McGregor et al. (2014) later proposed as a cause of the Pacific intensification the

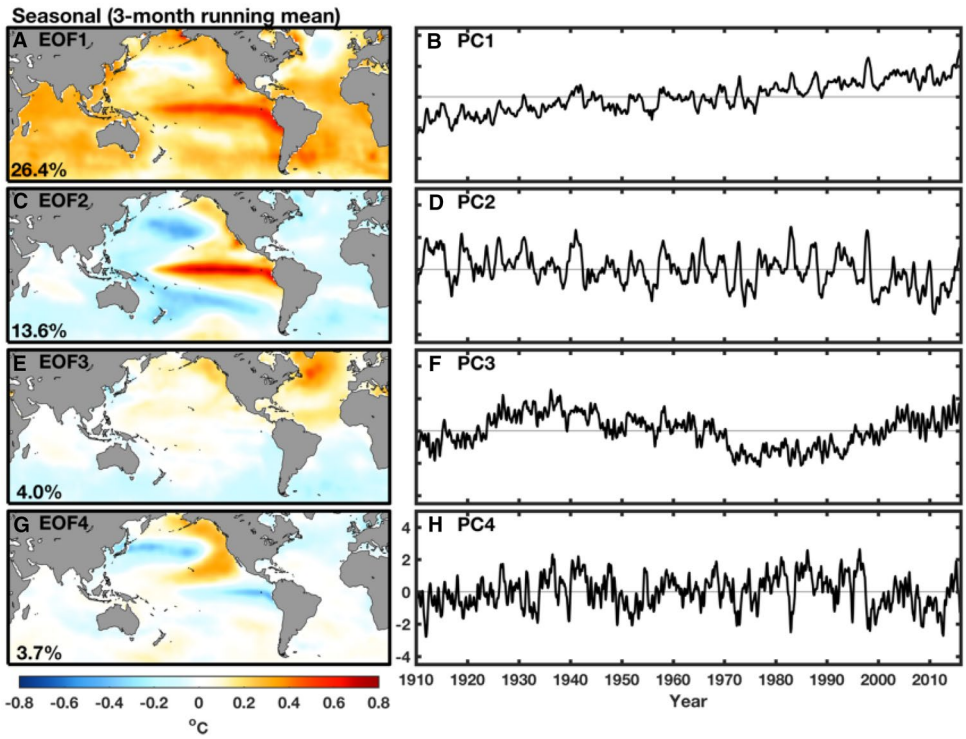

Fig. 15 Conventional EOF analysis of global SST

convection due to the warming SST in the Atlantic. Li et al. (2016) reaffirmed that the observed tropical Atlantic SST warming could cause an enhanced Walker circulation, accompanied by the warming of Indo-western Pacific Ocean, and the cooling of the eastern Pacific. The results from these "nudging" experiments should be interpreted with care (see Tung and Chen 2018): the location where the observed SST is imposed in these experiments is not necessarily the cause of the change in the freely evolving Pacific. This pan-tropics warming may be part of global warming.

Our work of explaining the events as they were observed does not involve this controversy related to models. Nevertheless, a projection of the future state of the Central Pacific is highly uncertain unless this issue is understood. The study of the CP El Niño and the relationship of our CPV mode to the observed trade wind changes may help resolve this larger controversy on the response to anthropogenic forcing.

Acknowledgements YF was supported by Natural Science Foundation of China under Grant 41776027 and China Scholarship Council during her exchange study at University of Washington, when the work reported here was carried out. This forms part of her Ph.D. thesis under Prof. JY Hu, who provided advice and support. XC was supported by the Natural Science Foundation of China under Grants 41825012 and 41776032 and the Natural Science Foundation of China-Shandong Joint Fund for Marine Science Research Centers under Grant U1406402. KKT was supported in part by the Frederic and Julia Wan Endowed Professorship and by National Science Foundation, under NSF1536175 and AGS-1262231.

Appendix: trend transfer in pairwise rotated PCA

As described in CWT, a trend transfer procedure is adopted whereby the trends in $prPC_j$ with j = 2, 3, 4,…., which are called dynamical modes, are transferred to $prPC_1$, which contain all the trends, including that from global warming. The transfer is done pair by pair. The rationale for needing to do such a trend transfer is given below.

In the SST and surface temperature data in the industrial era, there exists a (non-uniform) global warming trend. In a conventional EOF analysis, this trend shows up in the leading PC, PC_1, due to its high variance. This is shown in Fig. 15. This PC_1 is practically the same as the global mean SST. Its spatial pattern (EOF_1) is practically the same as that obtained by regressing the SST onto this time series, and is warming almost everywhere but with some features. The higher modes, called dynamical modes, are required to be orthogonal to it in both their PC and EOF, creating some artifacts. This can be seen in the figure. Note for example, that PC_2, the ENSO-like mode, contains a negative trend, so that the trends of the two PCs yield a negative correlation, which cancels the positive correlation of the non-trend parts of the time series. In the spatial domain, the tropical warm tongue associated with tropical ENSO in EOF2 yields a positive covariance with a similar feature in EOF1, which balances with negative covariance elsewhere. Similarly there is also a mode mixing related to the AMO in the North Atlantic, whereby a

positive trend is generated in PC_3. These features may or may not be associated with physical modes.

In prPCA, we relax the constraint that the EOFs be orthogonal with each other. If they still turn out to be orthogonal that may indicate that the physical modes possess such a property. Usually they do not turn out to be orthogonal. We still require the prPC's be orthogonal to each other, but we shall require such orthogonality not be accomplished through the generation of an artificial trend in the dynamical PCs. We shall assume that the modes associated with internal variability do not have a secular trend.

This type of mode mixing (one that is associated with trends) can be eliminated by trend transfer, which is also a pair-wise rotation of PCs.

The rotation of a pair of PCs through an angle θ is given by the following formula:

$$prPC_i = \cos\theta PC_i - \sin\theta PC_j$$
$$prPC_j = \sin\theta PC_i + \cos PC_j$$

where $i=2, 3, 4$, etc., and $j=1$. We shall use $i=2$ for illustration below. Let

$$PC_1 = k_1 t + b_1(t), \quad PC_2 = k_2 t + b_2(t)$$
$$prPC_1 = m_1 t + n_1(t), \quad prPC_2 = m_2 t + n_2(t).$$

The b's and n's are assumed to have no linear trend. After rotation we want $m_2=0$. Therefore

$$k_2 \cos\theta = k_1 \sin\theta = 0$$
$$n_2(t) = b_2(t)\cos\theta - b_1(t)\sin\theta$$

Hence:

$$\tan\theta = \frac{k_2}{k_1}.$$

That is, the required rotation angle is given by the arctangent of the ratio of the slope sof PC_2 and PC_1.

It can be shown that if sufficient resolution were used in the EOF analysis (over 1000 PC's), the first mode, $prPC_1$ would become simply a linear trend after over 1000 trend transfers. Therefore, this procedure would be equivalent to first linearly detrending the SST and then doing the EOF analysis. However, global warming is not necessarily linear, although it may be approximately so after 1910 after the removal of ENSO and AMO contributions (see Chen and Tung 2018). Furthermore, the modes that make $prPC_1$ smoothly linear are very small-scale fluctuations. With the small number of EOFs used in our analysis, $prPC_1$ still contains dips that can be identified with volcanic eruptions, and the change in SST measurement methods near the end of WWII. These are in the real data and should not be buried in very high modes.

References

Ashok K, Yamagata T (2009) Climate change: the El Niño with a difference. Nature 461:481

Ashok K, Behera SK, Rao SA, Weng H, Yamagata T (2007) El Niño Modoki and its possible teleconnection. J Geophys Res Oceans 112:C11007

Buell CE (1979) On the physical interpretation of empirical orthogonal functions. In: Preprints sixth conference on probability and statistics in atmospheric sciences, Banff, Alta. American Meteorological Society

Cai W et al (2015) ENSO and greenhouse warming. Nat Clim Change 5:849

Cane MA et al (1997) Twentieth-century sea surface temperature trends. Science 275:957–960

Capotondi A et al (2015) Understanding ENSO diversity. Bull Am Meteor Soc 96:921–938

Chen X, Tung K-K (2018) Global-mean surface temperature variability: space–time perspective from rotated EOFs. Clim Dyn 51:1719–1732

Chen X, Wallace JM (2016) Orthogonal PDO and ENSO indices. J Clim 29:3883–3892

Chen X, Wallace JM, Tung K-K (2017) Pairwise-rotated EOFs of global SST. J Clim 30:5473–5489

Choi J, An S-I, Yeh S-W (2012) Decadal amplitude modulation of two types of ENSO and its relationship with the mean state. Clim Dyn 38:2631–2644

Choi K-Y, Vecchi GA, Wittenberg AT (2013) ENSO transition, duration, and amplitude asymmetries: role of the nonlinear wind stress coupling in a conceptual model. J Clim 26:9462–9476

Clement AC, Seager R, Cane MA, Zebiak SE (1996) An ocean dynamical thermostat. J Clim 9:2190–2196

Dee DP et al (2011) The ERA-interim reanalysis: configuration and performance of the data assimilation system. Q J R Meteorol Soc 137:553–597

Di Lorenzo E et al (2008) North Pacific Gyre Oscillation links ocean climate and ecosystem change. Geophys Res Lett 35:L08607

Ding R, Li J, Tseng YH, Sun C, Guo Y (2015) The Victoria mode in the North Pacific linking extratropical sea level pressure variations to ENSO. J Geophys Res : Atmos 120:27–45

Ding Q, Steig EJ, Battisti DS, Wallace JM (2012) Influence of the tropics on the southern annular mode. J Clim 25(18):6330–6348

Eisenman I, Yu L, Tziperman E (2005) Westerly wind bursts: ENSO's tail rather than the dog? J Clim 18:5224–5238

England MH et al (2014) Recent intensification of wind-driven circulation in the Pacific and the ongoing warming hiatus. Nat Clim Change 4:222

Fedorov AV, Hu S, Lengaigne M, Guilyardi E (2015) The impact of westerly wind bursts and ocean initial state on the development, and diversity of El Niño events. Clim Dyn 44:1381–1401

Feng J, Wu Z, Zou X (2014) Sea surface temperature anomalies off Baja California: a possible precursor of ENSO. J Atmos Sci 71(5):1529–1537

Feng Y, Tung K-K (2019) ENSO modulation: real and apparent; implications for decadal prediction. Clim Dyn **(submitted)**

Giese BS, Ray S (2011) El Niño variability in simple ocean data assimilation (SODA), 1871–2008. J Geophys Res Oceans 116:C02024

Glantz MH, Glantz MH (2001) Currents of change: impacts of El Niño and La Niña on climate and society. Cambridge University Press, Cambridge

Han W et al (2014) Intensification of decadal and multi-decadal sea level variability in the western tropical Pacific during recent decades. Clim Dyn 43:1357–1379

Hu S, Fedorov AV (2018) Cross-equatorial winds control El Niño diversity and change. Nat Clim Change 8:798

Ishii M, Kimoto M (2009) Reevaluation of historical ocean heat content variations with time-varying XBT and MBT depth bias corrections. J Oceanogr 65:287–299

Ishii M, Shouji A, Sugimoto S, Matsumoto T (2005) Objective analyses of sea-surface temperature and marine meteorological variables for the 20th century using ICOADS and the Kobe collection. Int J Climatol 25:865–879

Ishii M, Kimoto M, Sakamoto K, Iwasaki S-I (2006) Steric sea level changes estimated from historical ocean subsurface temperature and salinity analyses. J Oceanogr 62:155–170

Johnson NC (2013) How many ENSO flavors can we distinguish? J Clim 26:4816–4827

Kao H-Y, Yu J-Y (2009) Contrasting eastern-Pacific and central-Pacific types of ENSO. J Clim 22:615–632

Kohyama T, Hartmann DL, Battisti DS (2017) La Niña-like mean-state response to global warming and potential oceanic roles. J Clim 30:4207–4225

Kug J-S, Jin F-F, An S-I (2009) Two types of El Niño events: cold tongue El Niño and warm pool El Niño. J Clim 22:1499–1515

Larkin NK, Harrison D (2005a) On the definition of El Niño and associated seasonal average US weather anomalies. Geophys Res Lett 32:L13705

Larkin NK, Harrison D (2005b) Global seasonal temperature and precipitation anomalies during El Niño autumn and winter. Geophys Res Lett 32:L16705

Lee T, McPhaden MJ (2010) Increasing intensity of El Niño in the central-equatorial Pacific. Geophys Res Lett 37:L14603

Lengaigne M et al (2004) Triggering of El Niño by westerly wind events in a coupled general circulation model. Clim Dyn 23:601–620

Li X, Xie S-P, Gille ST, Yoo C (2016) Atlantic-induced pan-tropical climate change over the past three decades. Nat Clim Change 6:275

Lian T, Chen D (2012) An evaluation of rotated EOF analysis and its application to tropical Pacific SST variability. J Clim 25:5361–5373

Mantua NJ, Hare SR, Zhang Y, Wallace JM, Francis RC (1997) A Pacific interdecadal climate oscillation with impacts on salmon production. Bull Am Meteor Soc 78:1069–1080

McGregor S, Timmermann A, Stuecker MF, England MH, Merrifield M, Jin F-F, Chikamoto Y (2014) Recent Walker circulation strengthening and Pacific cooling amplified by Atlantic warming. Nat Clim Change 4:888

McPhaden M, Lee T, McClurg D (2011) El Niño and its relationship to changing background conditions in the tropical Pacific Ocean. Geophys Res Lett 38:L15709

Newman M, Compo GP, Alexander MA (2003) ENSO-forced variability of the Pacific decadal oscillation. J Clim 16:3853–3857

Newman M et al (2016) The Pacific decadal oscillation, revisited. J Clim 29:4399–4427

North GR, Bell TL, Cahalan RF, Moeng FJ (1982) Sampling errors in the estimation of empirical orthogonal functions. Mon Weather Rev 110:699–706

Philander SGH (1983) El Niño southern oscillation phenomena. Nature 302:295

Rasmusson EM, Carpenter TH (1982) Variations in tropical sea surface temperature and surface wind fields associated with the Southern Oscillation/El Niño. Mon Weather Rev 110:354–384

Rayner N et al (2003) Global analyses of sea surface temperature, sea ice, and night marine air temperature since the late nineteenth century. J Geophys Res Atmos 108:4407

Ren HL, Jin FF (2011) Niño indices for two types of ENSO. Geophys Res Lett 38:L04704

Rodgers KB, Friederichs P, Latif M (2004) Tropical Pacific decadal variability and its relation to decadal modulations of ENSO. J Clim 17:3761–3774

Sarachik ES, Cane MA (2010) The El Niño-southern oscillation phenomenon. Cambridge University Press, Cambridge

Smith TM, Reynolds RW (2004) Improved extended reconstruction of SST (1854–1997). J Clim 17:2466–2477

Smith TM, Reynolds RW, Peterson TC, Lawrimore J (2008) Improvements to NOAA's historical merged land–ocean surface temperature analysis (1880–2006). J Clim 21:2283–2296

Sun F, Yu J-Y (2009) A 10–15-yr modulation cycle of ENSO intensity. J Clim 22:1718–1735

Takahashi K, Montecinos A, Goubanova K, Dewitte B (2011) ENSO regimes: reinterpreting the canonical and Modoki El Niño. Geophys Res Lett 38:L10704

Trenberth KE, Stepaniak DP (2001) Indices of el niño evolution. J Clim 14:1697–1701

Tung KK, Chen X (2018) Understanding the recent global surface warming slowdown: a review. Climate 6:82–100

Vecchi GA, Soden BJ, Wittenberg AT, Held IM, Leetmaa A, Harrison MJ (2006) Weakening of tropical Pacific atmospheric circulation due to anthropogenic forcing. Nature 441:73

Wang B, Liu J, Kim H-J, Webster PJ, Yim S-Y, Xiang B (2013) Northern hemisphere summer monsoon intensified by mega-El Niño/southern oscillation and Atlantic multidecadal oscillation. Proc Natl Acad Sci 110:5347–5352

Xiang B, Wang B, Li T (2013) A new paradigm for the predominance of standing central Pacific warming after the late 1990s. Clim Dyn 41:327–340

Yeh SW, Kirtman BP (2004) Tropical Pacific decadal variability and ENSO amplitude modulation in a CGCM. J Geophys Res Oceans 109:C11009

Yeh S-W, Kug J-S, Dewitte B, Kwon M-H, Kirtman BP, Jin F-F (2009) El Niño in a changing climate. Nature 461:511

Yu J-Y, Lu M-M, Kim ST (2012) A change in the relationship between tropical central Pacific SST variability and the extratropical atmosphere around 1990. Environ Res Lett 7:034025

Zhang Y, Wallace JM, Battisti DS (1997) ENSO-like interdecadal variability: 1900–93. J Clim 10:1004–1020

Publisher's Note Springer Nature remains neutral with regard to jurisdictional claims in published maps and institutional affiliations.